PALEOCEANOGRAPHIC MAPPING PROJECT
PROGRESS REPORT No. 40 - 0888

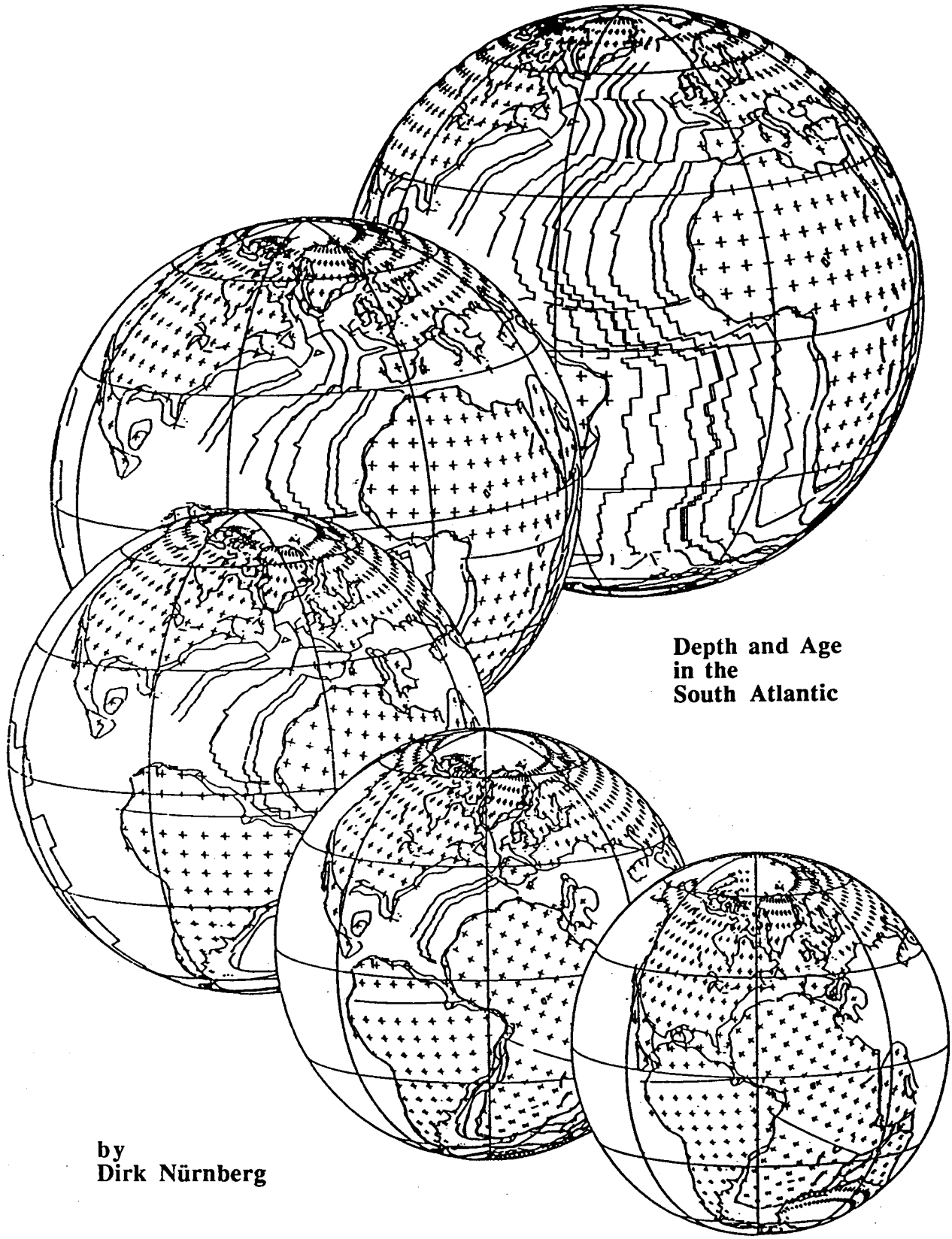

Depth and Age in the South Atlantic

by
Dirk Nürnberg

University of Texas Institute for Geophysics Technical Report No. 92

Depth and Age in the South Atlantic Ocean

Dirk Nürnberg

Institute for Geophysics, The University of Texas

Abstract

A significant flattening of the relation between depths and age of ocean floor older than 80 Ma can be explained by assuming that the oceanic lithosphere acts as a thermal boundary layer on top of a viscous upper mantle. In the past, uncertainties of age, of sediment thickness and of bathymetry limited the predictions about this relationship. In this study, recent data from the South Atlantic have been averaged into half by half degree elements, so that the relationship between depth and age can be studied in detail. We constructed a high resolution isochron chart for the South Atlantic using the latest available compilation of magnetic anomaly data and satellite altimetry data. The most recent sediment thickness map is used to correct bathymetry for sediment loading in order to obtain the accurate depth to basement. We have plotted the corrected basement depth versus age for the entire South Atlantic as well as for distinct areas. The depth/age relationship is presented as contours about the mode enclosing approximately two thirds of the data. In the South Atlantic, the ocean floor subsides with the square root of age on crust younger than 80 Ma. Beyond 80 Ma depths flatten significantly with age. Moreover, a change of the depth/age relationship for opposite flanks as well as with latitude is obvious, which might be related to small scale convection in the upper mantle.

Introduction

Oceanic lithosphere is created at spreading centers by the intrusion of hot molten basaltic material. The newly formed material accretes to the already existing oceanic crust and with the emplacement of more basalt moves away from the spreading axis. During this process, the new oceanic lithosphere cools and contracts. Thus, hot and shallow ocean floor appears near the ridge axis and becomes colder and deeper with increasing distance from the ridge. Since the relationships between heatflow and age and depth and age

represent, ideally, the cooling behavior of a thermal boundary layer, they can be used to constrain the exact nature of this layer (Renkin and Sclater, 1988).

Two models have been proposed to account for the variation in depth and heatflow with increasing age of the ocean floor (Figure 1). In the one-layer simple cooling, square root of age model of the lithosphere, the thermal boundary layer consists of a single layer that thickens linearly with the square root of age as it cools by conduction (Turcotte and Oxbrugh, 1967; Parker and Oldenburg, 1973). The oceanic depth increases with the square root of age and the heat flow decreases with one upon the square root of age (Davis and Lister, 1974). However, the average depths of the ocean floor older than 80 Ma do not increase as predicted (Parsons and Sclater, 1977). Crough (1978) and Heestand and Crough (1981) attempted to explain the observed flattening of the depth curve by thermal anomalies in the upper mantle. Hot spots might thin the cooling boundary layer and create broad regions of shallower than expected depths (Crough, 1978; Heestand and Crough, 1981).

To account for the observed flattening of the depth/age curve of old oceanic crust, Langseth et al. (1966), McKenzie (1967) and Parsons and McKenzie (1978) proposed a model, where the boundary layer consists of a flat plate, and depth and heat flow decrease exponentially to a constant value. This single boundary layer consists of a rigid mechanical layer and a thermal boundary layer which separates the rigid mechanical layer from the viscous asthenosphere. The thermal boundary layer is stable near the spreading axis. As the lithosphere moves away from the spreading ridge, both the rigid mechanical layer and the thermal boundary layer thicken. However, if the thermal boundary layer exceeds a critical value, it becomes unstable and causes convection, which brings additional heat to the base of the mechanical layer (Renkin and Sclater, 1988). This additional heat flux prevents the layer from increasing in thickness. Thus, the depth flattens exponentially to a constant depth. Within this two-layer, thermo-mechanical, 'plate' model, regions of positive anomalous depth are explained by the upwelling limbs of convection cells in the upper mantle. The upwelling limb thins and uplifts the lithosphere when penetrating the thermal boundary layer. However, convective limbs do not explain the overall flattening of the depth profile (Renkin and Sclater, 1988).

Only few authors have worked on the depth/age relationship in the South Atlantic, which is mainly due to the sparse database concerning age, bathymetry and sediment thickness. Sclater and McKenzie (1973) created paleobathymetric charts of the South Atlantic based primarily on a depth/age relationship they derived from DSDP-sites in the North Atlantic and Pacific. Hayes (1988) compared the depth and age of the ocean floor for the entire South Atlantic using bathymetry, sediment thickness and age data averaged

for one by one degree intervals. Hayes' study, however, is limited, since Ladd's (1974) isochrons for the South Atlantic were used.

In this study, the depth/age modelling is restricted to a region between the equator and 55°S, since age, depth and sediment thickness are only well-constrained in this area of the South Atlantic. We developed a high resolution isochron chart for the South Atlantic based on a recent compilation of magnetic anomaly picks and lineations (Cande et al., in press; Rabinowitz and LaBrecque, 1979; Martin et al., 1980). This map served to compute the mean age of ocean floor at the center of each half by half degree element. Depth to seafloor averaged for each half by half degree element was derived from the digitized topographic and bathymetric ETOPO5 database (NOAA). In order to yield depth to the top of the oceanic crust at each element, we corrected the bathymetry for sediment loading by applying the Crough-correction (Crough, 1983). Our sediment thickness data are based on the latest available sediment thickness map of the South Atlantic, compiled by Divins and Rabinowitz (in press). The depth/age relationship for the South Atlantic ocean crust was examined for the entire area as well as for distinct parts of the ocean basin in order to examine subsidence behavior for different parts of the South Atlantic ocean floor. Results are shown as contours around the mode according to a method developed by Renkin (1986). Residual depth anomalies were compared to the intermediate wavelength geoid height (Sandwell and McKenzie, in prep.) to evaluate an origin of depth anomalies beneath the lithosphere.

A revised isochron chart for the South Atlantic

The general tectonic evolution of the South Atlantic is well known, since Dickson et al. (1968) constructed the first isochrons for the South Atlantic. Ladd (1974) determined the relative motion of South America with respect to Africa from Early Cretaceous to present day from the magnetic anomaly pattern and published finite rotation poles between North America and Africa (Pitman and Talwani, 1972). Ladd's isochrons for the South Atlantic were improved by Larson et al. (1985), who incorporated Seasat altimetry data in addition to the magnetic anomalies to determine ridge crest offsets and locations of poorly known fracture zones. Cande (in press.) compiled a tectonic map of the South Atlantic, showing the location of fracture zones, sea floor spreading magnetic anomalies and the ridge axis (Figure 2). To derive an improved high resolution isochron chart for the South Atlantic, we combined magnetic anomaly data with satellite altimetry data (Figure 3).

Satellite altimetry data

Gahagan et al. (1988) derived a tectonic fabric map for the South Atlantic ocean floor from Seasat altimetry data used in the form of the "along track deflection of the vertical" (Sandwell, 1984). The processing technique of the Seasat data is discussed in Gahagan et al. (1988). The tectonic fabric map of the South Atlantic, based on the first derivative of the measured sea surface, delineates features such as fracture zones, volcanic ridges, marginal basins and seamounts. Blue and red lines represent maximum positive and negative linear gradients in the geoid, as viewed to northeast, whereas hatched areas reflect less steep, broad zones of geoid anomalies. The relation between the observed geoid signal and fracture zones, however, depends on various aspects: 1) the fracture zone's morphology, 2) the spreading rate of the adjacent ridge axis, and 3) the age offset across the fracture zone (Gahagan et al., 1988).

A simple morphologic model of fracture zones represented by steps in the basement is seldom in accordance with bathymetric and gravimetric data over fracture zones (Collette, 1986). Usually, fracture zones exhibit a more complex morphology, mostly due to variations in seafloor spreading velocity and direction, as well as age offset. Small age offset, slow spreading fracture zones clearly show a different geoid signal than large age offset, fast spreading fracture zones due to different morphology (Gahagan et al., 1988). Closely spaced pairs of red and blue Seasat lineations are characteristic of the South Atlantic, implying that the seafloor morphology deepens and then flattens again. Therefore we assume central bathymetric valleys, typical for slow spreading, rather than basement steps to be the most common morphologic features of South Atlantic fracture zones. Gravity and bathymetric measurements along the western portion of the Rio Grande Fracture Zone confirm the trough-like nature of this fracture zone (Gamboa and Rabinowitz, 1981).

The geoid lineations interpreted from Seasat altimetry data for the South Atlantic usually are interrupted and discontinuous. The data in the Argentine, Brazil, Cape and Angola Basins are particularly sparse. Only some prominent fracture zones show relatively continuous pairs of red and blue lineations that can be traced over broad distances of the ocean floor. These are the Ascension, Bode Verde, Rio de Janeiro, Rio Grande, Tristan de Cunha, Gough and Falkland-Agulhas fracture zones.

Interpretations of the more recent Geosat altimetry data resulted in a much improved map of geoid lineations in the South Atlantic (Nürnberg et al., in prep.). As expected, the location of prominent positive and negative geoid gradients is similar to the Seasat derived lineations, though Geosat data clearly allow a continuous interpretation of fracture zone

lineations over much broader areas. Geosat altimetry data provide an excellent means to better identify fracture zone locations, which resulted in a reinterpretation of the tectonic development in the Agulhas Basin, (Nürnberg et al., in prep.).

Magnetic anomaly data

The relative motion history between South America and Africa from about 130 Ma to present day was reconstructed from a recent compilation of magnetic anomaly picks and lineations in the South Atlantic (Cande et al., in prep.; see also Barker, 1979; LaBrecque and Hayes, 1979; Rabinowitz and LaBrecque, 1979; Martin et al., 1982). Ages of magnetic anomalies were taken from the time scale of Kent and Gradstein (1986). Magnetic anomaly pick locations for A34 to A3 correspond to the young end of the normal polarity interval (Cande et al., in press). In the Agulhas Basin (Barker, 1979; LaBrecque and Hayes, 1979), magnetic picks are defined by the old end of the normal polarity interval. Magnetic anomaly data in the Agulhas Basin were partly reinterpreted using profiles from Barker (1979) and LaBrecque and Hayes (1979).

Cande et al. (in press.) calculated 45 finite rotation poles between Chron A34 and Chron A3, each representing an average time interval of less than 2 Ma. Most of Cande et al. 's (in press.) poles satisfy the data constraints. The poles for magnetic anomalies 6a, 6c, 11, 16, 20, 25, however, were slightly modified. The 3D graphic capabilities of an interactive Evans and Sutherland computer system were used to find new poles and to check previously published finite rotation poles that best fit corresponding magnetic anomalies and fracture zone lineations from both sides of the mid-ocean ridge.

In addition to finite rotation poles fitting magnetic lineations for Chron A34 to Chron A3, finite poles of rotation for Chron M0 and Chron M4 were derived by taking into account intracontinental deformation within South America and Africa during the early opening phase of the South Atlantic. The derivation of the M0 and M4 poles are based on magnetic anomaly picks and lineations in the southernmost South Atlantic published by Rabinowitz and LaBrecque (1979), Barker (1979), LaBrecque and Hayes (1979), Martin et al. (1982) and Cande et al. (in press.).

Construction of isochrons

Isochrons for each stage were derived by rotating corresponding magnetic anomaly picks together by holding one of two plates fixed. We then drew isochron segments by defining the best average line through a reconstructed set of magnetic anomaly picks.

Subsequently,we produced a duplicate of the isochron and rotated it to the other side of the ridge by applying the same pole of rotation that had been used for the reconstruction. The single isochron segments were connected by transform fault segments, whose locations were defined by pairs of red and blue geoid lineations, particularly when magnetic data were sparse. Where magnetic data as well as geoid data are lacking, the fracture zones were constructed by comparison to younger and older isochrons. The directions of the isochron offsets were drawn according to small circles about each stage pole. This resulted in synthetic flowlines. Large areas of the southernmost South Atlantic ocean floor were created during the Cretaceous Quiet Zone, consequently lacking any magnetic signals. However, when gridding the isochron map of the South Atlantic, we assigned ages to each half by half degree element by linearly interpolating between Chron 34 and Chron M0, assuming a constant spreading rate during the Cretaceous Quiet Period. The same linear interpolation of ages is applied north of the Rio Grande Rise/Walvis Ridge system between isochron A 34 and the continental margin.

Bathymetry (Depth of the Seafloor)

The digitized ETOPO5 data set of world elevations compiled by NOAA provides the basic data set for the South Atlantic bathymetry. The bathymetric data are corrected for the ocean-wide variation of the velocity of sound in seawater (Matthews, 1939) and are averaged from 5 minute to half degree intervals. When contoured, the resulting bathymetric data set shows all major bathymetric features in the South Atlantic (Figure 4). The depth increases symmetrically from the mid-ocean ridge to both the African and South American sides, interrupted by the Rio Grande Rise, the Walvis Ridge, Meteor Rise, Islas Orcadas Rise, Ascension Island and Discovery Island. The Argentine, Brazil, Cape and Angola basins are the deepest areas in the South Atlantic.

Sediment thickness

Divins and Rabinowitz (in press.) constructed the most recent chart of sediment thickness for the South Atlantic (Figure 5). Approximately 315,000 km of single channel seismic profiles as well as sonobuoy reflection/refraction profiles were used to derive sediment thickness in two-way travel reflection time. The data were converted into thickness in kilometers, using different velocity regression equations. The results were averaged in 100 km intervals along the cruise tracks before being contoured. We compared the sediment thickness shown on the map to depth to basement as determined after data

from DSDP-drilling sites. The agreement of both data sets is satisfactory for most sites. We present the sediment thickness of the South Atlantic in two-way travel reflection time converted from kilometers, using the same velocity regression equations as Divins and Rabinowitz (in press) (Figure 6).

The distribution of sediments shows a simple pattern. Sediment thickness generally increases with increasing distance from the spreading center. However, within about 1000 km on either side of the ridge, sediments are mostly less than 100m thick (Divins and Rabinowitz, in press). The Argentine Basin has a sediment thickness of about 3 km, whereas the Angola, Cape, and Brazil basins generally have less than 1 km sediment thickness. The greatest amount of sediments, up to about 10 km, can be found in marginal basins on the continental shelves. These sediments, however, are not included into our study because they lie on continental crust.

Correction of Depth to Basement for Sediment Loading

It is necessary to correct the observed seafloor depth for sediment loading when investigating subsidence and uplift of oceanic crust (Sclater et al., 1971; Menard, 1973, Crough 1983). For a thin sediment cover, it is sufficient to assume that sediment density and velocity are constant valued with both depth and lateral position. However, on old seafloor the sediment cover generally exceeds 1 km of thickness, requiring a more accurate sediment correction.

Crough (1983) found a simple linear relationship between two-way sediment reflection time and the correction for sediment loading which will correct seafloor depth to get basement depth in the absence of sediment loading. This relationship is mainly derived from DSDP-sites drilled in the North Atlantic. We checked the Crough-relationship by using sediment parameters derived from 10 DSDP-sites in the South Atlantic (Figure 7). Sediment correction and two-way travel time are calculated from depth, velocity and sediment density. All DSDP-sites examined show a linear relationship between two-way travel time and sediment correction.

To compute depth to basement corrected for sediment loading, we first digitized the sediment thickness map in two-way travel time at half by half degree intervals. Each value is then multiplied by the Crough-correction factor of 600m/s (slope of the linear relation between the sediment correction and two-way travel time). The resulting value is finally added to the bathymetric depth given by the ETOPO5 database.

This method works well as long as depth to acoustic basement given by the sediment thickness map corresponds to the actual top of the ocean floor. In the case of

substantial volcanism after the creation of oceanic crust, which would result in basaltic flows and sills intercalated with the sediments, the method is not accurate. These intrusions cause an additional loading effect which would have to be considered in the calculation (Renkin and Sclater, 1988). In the South Atlantic we assume the acoustic basement to be the actual top of the ocean floor, as we have no evidence for intercalations of basalt flows or sills in the sediment pile.

Depth versus age

Since magnetic anomalies in the South Atlantic are reasonably well-preserved on both sides of the spreading axis and bathymetry and sediment thickness is quite well-known, this ocean basin is ideal for depth/age modelling. The updated database digitized at half by half degree intervals improves the accuracy of the depth/age plots and allows new insights into the subsidence of oceanic lithosphere. In our study, we excluded all data on continental crust, defined as the area on the continental shelves seawards between the coastline and the continental-oceanic crust boundary (COB) from Emery and Uchupi (1984). We slightly modified the COB between 20°S and 30°S by interpretation of Seasat altimetry data (Nürnberg et al., in prep.). Emery and Uchupi (1984) mapped the seaward edge of the South American salt basins as the COB. However, Seasat lineations give clear evidence for a large part of the salt being deposited or mobilized onto oceanic crust.

There is no reason to present the observations in decreasingly constrained steps as Renkin and Sclater (1988) did for areas in the North Pacific differentially constrained by the data. However, we show depth/age plots for different areas in the South Atlantic to clarify regional differences in subsidence of oceanic lithosphere. Each data point plotted represents the value determined for each single half by half degree element (Figures 8, 10, 11, 12, and 13). The distribution of depth with age shows significant scatter in all plots, especially where the depth levels of crust older than 80 Ma. Moreover, the relationship between depth and age is skewed due to volcanic features. It is difficult to remove the effect of volcanic features from the calculation, because the point where a seamount blends into the surrounding ocean floor is a matter of conjecture. In addition, the flexural moats around the seamounts have to be considered, though these are even less well-defined (Renkin and Sclater 1988). Mean and standard deviation poorly represent the data because of this skewness. Consequently, we present the data as contours around the mode as suggested by Renkin and Sclater (1988). They found that a contour enclosing approximately two thirds of the points best represents the data.

Depth/age relationship for all data examined

In Figure 8 we plot depth against age for all data sampled in the South Atlantic. Though there is significant scatter in the data, there is strong evidence for a uniform subsidence from present day to at least 80 Ma, which is predicted by the simple cooling model and the plate model. However, for crust older than 80 Ma the data show a general flattening of depth with age, being in closer accordance with the thermo-mechanical plate model. On older crust, the amount of scatter in the data increases. At the same time, the depth/age relationship is skewed (Figure 9), mainly due to the inclusion of seamounts and volcanic features like the Rio Grande Rise and the Walvis Ridge into the data set. However, the contours around the mode (Figure 8c) clearly show that the observed depth of oceanic crust corresponds to both thermal models at least up to 80 Ma. After 80 Ma the thermo-mechanical plate model better fits the flattening trend of the data.

All data except Rio Grande Rise and Walvis Ridge

In order to determine the reason for the obvious scatter in the data, especially on older seafloor, we removed the data from the most significant volcanic features from our calculation. These features are the Rio Grande Rise and the Walvis Ridge, arbitrarily defined by the 4000m isobath. Here, we do not consider the flexural moats caused by this excess volcanism. In general, there is no great difference to the depth/age plot for all data (Figure 10). The scatter in data is less significant and the contours around the mode do not differ from the plot showing all data. The depth/age relation favors the thermo-mechanical plate model for crust older than 80 Ma, whereas for younger crust both the thermo-mechanical, "plate" model and the simple cooling model apply.

Western and eastern South Atlantic

To detect any differences in the depth/age relation for oceanic crust on both sides of the mid-ocean ridge, we have divided our data set according to the South American and the African plate. The depth versus age plot for the African plate clearly shows a good correlation to the simple cooling model and the plate model down to 80 Ma (Figure 11). On older crust, the depth flattens with age. The high scatter of data older than 80 Ma visible in the plots for mean and standard deviation (Figure 11b) is probably due to the South Atlantic aseismic ridges and seamounts, which have not been excluded.

For the South American plate the depth of oceanic crust younger than 80 Ma corresponds quite well to the Parsons and Sclater (1977) curves (Figure 12). Older crust, however, does not flatten similarly to the African crust of the same age, but lies deeper. A comparison of the contours around the mode for both African and South American plates clearly shows the African oceanic crust to be systematically shallower than the corresponding crust on the South American plate. Oceanic crust belonging to the South American plate, even crust older 80 Ma, clearly behaves as predicted by the two thermo-mechanical models. Surprisingly, for ages older than 80 Ma, the data lie in between the curves for the simple square root of age and the plate model. In contrast, oceanic crust in the eastern South Atlantic is generally shallower. Even at very young ages oceanic crust mainly lies higher than the predicted curves.

Argentine Basin

Heestand and Crough (1981) state that hot spots located both mid-plate and on mid-ocean ridges can bias the empirical depth/age relation. According to Schroeder (1984), ocean floor is influenced within 800 km of hot spot tracks due to heat flux from the mantle. Heestand and Crough (1981) suggest hot spots to be responsible for such a heat flux. To check, if the depth/age relationship predicted by the simple cooling and plate models holds for ocean crust both older than 80 Ma and distant from hot spot tracks, we extracted the data for the Argentine Basin (Figure 13). This basin is anomalously deep and seafloor is as far as 2200 km away from a hot spot track (Heestand and Crough, 1981). A map of hot spot tracks in the South Atlantic was published by Duncan (1981).

The depth of old oceanic crust in the Argentine Basin is in accordance with the thermo-mechanical models predicted by Parsons and Sclater (1977). Though the scatter of the data is wide, the mean clearly shows good correspondence to the simple square root of age model. The contours around the mode exhibit the oceanic crust of the Argentine Basin to be slightly deeper than predicted (Figure 13).

Five degree oceanic crust strips

The depth/age relation for oceanic crust differs significantly for both the South American and the African side. To prove if the depth/age relationship also shows changes by latitude, we have divided our data set according to single 5 degree strips of oceanic crust, reaching over the entire width of the South Atlantic. In addition, for each strip we

distinguished between data belonging to the African and to the South American plate (Figure 14).

It is obvious from these plots that the African oceanic crust is shallower than crust on the South American side. Figs. 15 and 16 exhibit the mean and standard deviations for both flanks of each oceanic crust strip. Plots showing the contours around the mode for each 5 degree strip confirm a change with latitude in addition to the differences of the depth/age relationship on both the South American and African flanks (Figs. 17). Apparently, oceanic crust in the South Atlantic does not behave according to one specific depth/age relationship.

However, we are able to classify the 5 degree strips of oceanic crust being in accordance with Hayes (1988). Between 5°S and 20°S the contour around the mode for the South American flank gives a good correlation to the theoretical model for about the last 40 Ma. Between 40 Ma and 80 Ma, the crust is significantly deeper than predicted, whereas crust older than 80 Ma flattens over the proposed subsidence curves. The corresponding crust on the African side is generally shallower, though the depths follow a linear relation. Beyond 80 Ma, however, the depths deviate significantly from the theoretical models.

Between 20°S and 35°S, the depths for a given age coincide quite well on both flanks, implying a symmetric subsidence history. A correlation to the thermo-mechanical models for both the South American and African oceanic crust younger than 80 Ma is obvious. Data for crust older than 80 Ma, however, scatter widely and depths are much shallower than predicted. The area described includes the data for the Rio Grande Rise and the Walvis Ridge, which probably causes the wide scatter of data on older crust.

The ocean floor between 35°S and 50°S is situated mainly south of the Rio Grande Rise/Walvis Ridge system. In this area, oceanic crust on the South American flank shows the best correlation to the simple, square root of age and plate model for all ages. Only depths between 45°S and 50°S are generally deeper than predicted. This coincides to the depth/age plots for the Argentine Basin (Figure 13). In contrast, oceanic crust on the African flank between 35°S and 50°S is much shallower than the thermo-mechanical models predict, even for ages younger than 80 Ma. In this southernmost part of the South Atlantic, depths on both flanks differ significantly, suggesting that the oceanic crust on the African plate must be influenced by some mechanism not effective for the corresponding South American side.

Residual depth anomalies in comparison to the geoid height

The simple age/depth relationship counts for about 60% of the oceanic crust, whereas the remaining portion of the oceanic seafloor deviates from this (Sclater et al., 1985). Oceanic areas, which obviously do not follow the subsidence curve outlined by Parsons and Sclater (1977) are called residual depth anomalies, which comprise mainly aseismic ridges and mid-ocean swells. The residual depth is defined as the difference between the observed depth corrected for sediment load and the expected depth from some relation between depth and age (Renkin and Sclater 1988). Depth anomalies generally lie more than 400m either above or below the depth predicted by the depth/age relationship.

The first type of depth anomaly, namely elongated regions of aseismic ridges (e.g. Ninetyeast Ridge, Walvis Ridge), is thought to be the result of excess volcanism on the ocean floor, either developed close to the mid-ocean ridge during the creation of oceanic crust or as off-ridge axis volcanism (Sclater et al., 1985). In general, it is associated with a fracture zone or a pronounced offset in the magnetic lineation pattern of the ocean floor and is often generated at sea-level. This volcanic material travels passively with the oceanic plate and moves away from the mid ocean ridge as time increases. These areas subside at the same rate as the ocean crust to which they are attached.

Mid-ocean swells without any relationship to either fracture zones or offsets in magnetic lineations exhibit the much broader, second type of depth anomalies. The Hawaiian Swell is an example of this type of depth anomalies and may be related to upwelling thermal convection cells in the upper mantle (Sclater et al., 1985). According to Crough (1978) and Parsons and Daly (1983), the effective thermal thickness of the plate is reduced by such convection cells. At the same time, the probability of volcanism and possible dynamical uplift of the plate increases.

To obtain a map of the residual depth anomalies in the South Atlantic, we subtracted the depths predicted by the thermo-mechanical models from those observed and contoured the residual depths at 500m intervals (Figure 18). A negative depth anomaly indicates a crustal depth shallower than predicted for its age. Positive depth anomalies indicate crust deeper than expected. At the ridge axis, depth anomalies range around $\pm$500m. The Rio Grande Rise and the Walvis Ridge as well as the Abrolhos Bank and Ascension Island appear as distinct negative depth anomalies. The largest positive depth anomalies (between +500m and +1000m) are in the Argentine Basin. We smoothed the residual depths using a low-pass Gaussian filter, which removes wavelengths shorter than 600 km (Figure 19). The main features in the South Atlantic, such as the Rio Grande Rise, the Walvis Ridge,

and the Falkland Plateau, still show distinct negative anomalies indicating that the ocean crust is shallower than predicted.

Haxby and Turcotte (1978) used the relationship between geoid height and topography to define the mode of isostatic compensation of a specific plateau or swell at intermediate wavelengths. Shallow Airy compensation exists if the ratio of geoid height to topography is low. An intermediate ratio is due to deeper compensation that can be attributed to lithospheric thinning (Crough 1978) and/or dynamic uplift from the rising limb of a convection cell (Parsons and Daly, 1983). A high ratio of geoid height to topography is caused by density anomalies beneath the lithosphere that are dynamically maintained by mantle convection (McKenzie et al., 1980). Several studies comparing the residual geoid height to topography observed a regular pattern of geoid heights and lows with a characteristic wavelength of 3000-4000km (Bowin and Thompson, 1984; Kogan et al., 1985; Marsh and Marsh, 1976; McKenzie et al., 1980; Watts and Daly, 1981; Marsh et al., 1984; Watts and Ribe, 1984; Watts et al., 1985). The regularity of the pattern as well as the bad correlation to topography was explained as being due to mantle convection (McKenzie et al., 1980). However, Sandwell and Renkin (1988) showed that the regular pattern of geoid highs and lows is artificially caused by improperly removing the longer wavelength reference geoid. Their processing removes the regular pattern, leading to a good correlation between geoid highs and lows and topographic highs and lows.

To determine the mode of compensation for distinct ocean floor features, we compared the smoothed residual depths to the geoid signal. We averaged the gridded geoid heights from quarter degree intervals into half degree intervals and removed wavelengths greater than 4000 km (Figure 20). The visual comparison of the smoothed residual depths and the geoid highs and lows indicates that there is a good positive correlation for the Rio Grande Rise, the Walvis Ridge and the Abrolhos Plateau off Brazil. Positive geoid signals correspond to oceanic crust lying shallower than predicted. In contrast, the residual depth anomalies for the Argentine Basin and the Brazil Basin clearly indicate that the basins lie deeper than predicted for their ages. The geoid heights show negative values. However, on the African plate, the relation between residual depths and geoid heights is skewed. Though the Angola and the Cape Basin show negative geoid signals, indicating geoid lows, the residual depths do not respond as one would expect. The Cape Basin clearly shows a negative value, indicating that this basin is shallower than predicted. Oceanic crust in the Angola Basin shows depths as predicted by the theoretical models, however, the geoid signal indicates a geoid low.

Discussion and conclusions

In the South Atlantic, the investigation of the relation between depth of oceanic basement to age clearly shows that the ocean floor younger than 80 Ma subsides linearly with the square root of age. However, oceanic crust older than 80 Ma significantly deviates from the relationship predicted by the simple, cooling, square root of age model. In contrast to Hayes (1988), we are able to show a flattening of the observed depths on crust older than 80 Ma. As the knowledge about age and sediment thickness in the South Atlantic is well-established, we think the flattening trend cannot be related to inaccuracies in these constraints. Since we have no evidence for substantial volcanism after the creation of oceanic lithosphere, which would increase the sediment loading, we do not consider this possibility in our calculation. Similar flattening of the oceanic lithosphere is reported from the North Pacific (Renkin and Sclater, 1988) and the western North Atlantic (Sclater and Wixon, 1986). Depths increases as a square root of age on crust between 0 and 80 Ma. Beyond 100 Ma, the depths deviate from the simple square root of age model and flatten significantly.

Heestand and Crough (1981) related the flattening trend to hot spots. The depths of ocean floor in the North Atlantic uninfluenced by hot spot tracks can satisfactorily be explained by the linear relationship of the square root of age model. Even oceanic lithosphere older than 80 Ma does not deviate from this relationship (Heestand and Crough, 1981). In fact, old ocean floor far away from any hot spot track exists only in the Argentine Basin between 45°S and 50°S. Here, the depths of the ocean floor correlate very well to the thermo-mechanical models and do not exhibit a flattening of data.

However, Renkin and Sclater (1988) do not relate the flattening trend of depths in the North Pacific beyond 80 Ma to Heestand and Crough's (1981) hot spot concept. They correlate the general flattening of depths with age to oceanic swells and valleys. The deviation from a linear relationship to an asymptotic curve indicates that the thermal boundary layer has reached equilibrium conditions under old ocean floor. This is expected, as any boundary layer in a system, where heat is input from below, has to flatten when equilibrium conditions are reached (Renkin and Sclater, 1988).

The depth/age relationship is shown separately for different areas in the South Atlantic. It is apparent from depth/age relationships for each flank of the South Atlantic spreading axis that the oceanic basement of the African plate is systematically shallower than on the South American plate. Hayes (1988) already mentioned this phenomenon in the South Atlantic. In order to investigate this relationship more closely, he subdivided the South Atlantic ocean floor into three latitudinal corridors, one of which being north of the

Rio Grande Rise / Walvis Ridge lineament, one of which being south of this lineament, and the third one including these aseismic ridges. Besides the different depth/age relationships on both sides of the mid-ocean ridge, Hayes (1988) showed a change of the crustal depth versus age relationship with latitude persisting throughout the entire evolutionary history of the South Atlantic. In this work, we show depth/age relationships for every 5 degree strips of ocean crust over the entire width of the South Atlantic. Moreover, we distinguished between South American and African plates. For each ocean floor strip, the contours around the mode clearly outline different depth behaviors with latitude and by plate. Strips showing asymmetric subsidence on both flanks may alternate with stripes of ocean crust showing symmetric subsidence. Obviously, mechanisms controlling the depth/age relationships can change abruptly within small areas. Hayes (1988) relates the regionally changing differences in subsidence rates to small differences in the temperature of the underlying asthenosphere, which might originate or be caused by small asthenospheric convection rolls oriented parallel to the spreading direction. However, Hayes (1988) gives no explanation to this problem.

The comparison of the residual depth anomalies and the geoid height in general shows a good correlation between the depths of oceanic crust and geoid highs and lows, respectively. However, the Angola Basin and the Cape Basin on the African plate deviate from this positive correlation. Both basins show a geoid low over crust, which is either too shallow (as in the Cape Basin), or which is at predicted depths (as in the Angola Basin).

Acknowledgements. I thank John G. Sclater for encouragement and guidance during this work. Furthermore, I would like to thank D. Divins, D. Hayes, D. Sandwell and S. Cande for providing necessary South Atlantic data, some of which were not published at the beginning of this study. C. Mayes, M. Renkin and D. McKenzie provided the computer programs and gave constructive advice. I like to thank V. Froger, N. Grindley, J.-Y. Royer and D. Müller for revising the manuscript and for thoughtful criticism. This work was supported by funding from Amoco International Oil Co., Chevron Overseas Petroleum Co., Conoco, Elf Aquitaine, Exxon Production Research, Mobil Oil Co., Petro Canada, Phillips Petroleum, Shell Development Co., and Standard Oil Co., as part of their sponsorship of the Paleoceanographic Mapping Project, University of Texas at Austin.

References

Barker, P.F., 1979. The history of ridge-crest offset at the Falkland-Agulhas Fracture Zone from a small-circle geophysical profile. Geophys. J. R. astr.Soc., 59: 131 - 145.

Bowin, C. and Thompson, G., 1984. Residual geoid anomalies in the Atlantic Ocean Basin: Relationship to mantle plumes. J. Geophys. Res., 89: 9905 - 9918.

Brozena, J.M.,1986. Temporal and spatial variability of seafloor spreading processes in the northern South Atlantic. J. Geophys. Res., 91(B1): 497 - 510.

Cande, S., LaBrecque, J.L., and Haxby, W.B., in press. Plate kinematics of the South Atlantic: Chron 34 to present. submitted to J. Geophys. Res.

Castro Jr., A.C.M.,1987. The northeastern Brazil and Gabon Basins: A double rifting system associated with multiple crustal detachment surfaces. Tectonics, 6(6): 727 - 738.

Chase, C.G., 1979. Subduction, the geoid, and lower mantle convection. Nature, 282: 464 - 468.

Collette, B.J., 1986. Fracture zones in the North Atlantic: morphology and a model. Jour. Geol. Soc., Lond., 14: 763 - 774.

Crough, S.T., 1978. Thermal origin of mid-plate hot-spot swells. Geophys. J.R. astro. Soc., 55: 451 - 469.

Crough, S.T., 1983. The correction for sediment loading on the seafloor. J. Geophys. Res., 88(B8): 6449 - 6454.

Crough, S.T. and Jurdy, D.M., 1980. Subducted lithosphere, hotspots, and the geoid. Earth and Planet. Sci. Let., 48: 15 - 20.

Davis, E.E. and Lister, C.R.B., 1974. Fundamentals of ridge crest topography. Earth Planet. Sci. Lett., 21: 405 - 413.

Dickson, G.O., Pitman III, W.C., and Heirtzler, J.R., 1968. Magnetic anomalies in the South Atlantic and ocean floor spreading. J. Geophys. Res., 73(6): 2087 - 2100.

Divins, D. and Rabinowitz, P., in press,

Duncan, R.A., 1981. Hotspots in the southern oceans - an absolute frame of reference for motion of the Gondwana continents. Tectonophysics, 74: 29 - 42.

Emery, K.O. and Uchupi, E., 1984. The Geology of the Atlantic Ocean, Springer, New-York, 1050 p.

Fairhead, J.D., in press. Mesozoic and Cenozoic plate tectonic reconstructions of the Central - South Atlantic Ocean: the role of the West and Central African Rift System.

Fairhead, J.D., Okereke, C.S., 1987. A regional gravity study of the West African rift system in Nigeria and Cameroon and its tectonic interpretation. Tectonophysics, 143: 143-159.

Gahagan, L.M., 1988, The mapping of tectonic features in the ocean basins from satellite altimetry data.- thesis, University of Texas at Austin.

Gahagan, L.M., Scotese, C.R., Royer, J.Y., Sandwell, D.T., Winn, J.K., Tomlins, R.L., Ross, M.I., Newman, J.S., Müller, R.D., Mayes, C.L., Lawver, L.A., and Heubeck, C.E., 1988. Tectonic fabric map of the ocean basins from satellite altimetry data. Tectonophysics.

Gamboa, L.A.P. and Rabinowitz, P.D., 1981. The Rio Grande Fracture Zone in the western South Atlantic and its tectonic implications. Earth Planet. Sci. Lett., 52: 410 - 418.

Grindley, N., in prep.. Temporal and spatial variations of magmatic segments along the Mid-Atlantic ridge (31°S - 34°S).

Gurnis, M., 1988. Large-scale mantle convection and the aggregation and dispersal of supercontinents. Nature, 33: 695 - 699.

Hager, H.B., Clayton, R.W., Richards, M.A., Comer, R.P., Dziewonski, A.M., 1985. Lower mantle heterogeneity, dynamic topography and the geoid. Nature, 313: 541 - 545.

Haxby, W.F. and Turcotte, D.L., 1978. On isostatic Geoid Anomalies. J. Geophys. Res., 83(B11): 5473 - 5478.

Hayes, D.E., 1988. Age/depth relationships and depth anomalies in the southeast Indian Ocean and South Atlantic Ocean. J. Geophys. Res., 93(B4):

Heestand, R.L. and Crough, S.T., 1981. The effect of hot spots on the oceanic age - depth relation. Jour. Geophys. Res., 86(B7): 6107 - 6114.

Kent, D.V. and Gradstein, F.M., 1986. A Jurassic to recent chronology.- in P.R. Vogt and B.E. Tucholke (eds.), The western North Atlantic region.- Geol. Soc. Amer., DNAG-Series, Vol. M, 45 -50.

Kogan, M.G., Diament, M., Bulot, A., and Balmino, G., 1985. Thermal isostasy in the South Atlantic Ocean from geoid anomalies. Earth Planet. Sci. Lett., 74: 280 - 290.

LaBrecque, J.L., and Hayes, D.E., 1979. Seafloor spreading history of the Agulhas Basin. Earth Planet. Sci. Letters, 45: 411-428.

Ladd, J.W., 1974. South Atlantic sea-floor spreading and Caribbean tectonics. Ph.D. thesis, 251pp., Columbia Univ., New York, 1974.

Langseth, M.S., LePichon, X., and Ewing, M., 1966. Crustal structure of mid-ocean ridges, 5, Heat flow through the Atlantic Ocean and convection currents. J. Geophys. Res., 71: 5321 - 5355.

Larson, R.L., Pitman III, W.C., Golovchenko, X., Cande, S.C., Dewey, J.F., Haxby, W.F., and LaBrecque, J.L., 1985. The bedrock geology of the world. Freeman, New York.

Marsh, B.D. and Marsh, J.G., 1976. On global gravity anomalies and two-scale mantle convection. J. Geophys. Res., 81: 5267 - 5280.

Marsh, B.D., Marsh, J.G., and Williamson, R.G., 1984. On gravity from SST, geoid from Seasat, and plate age and fracture zones. J. Geophys. Res., 89: 6070 - 6078.

Marsh, J.G., Brenner, A.C., Becklet, B.D., and Martin, T.V., 1986. Global mean sea surface based on the Seasat altimeter data. J. Geophys. Res., 91: 3501 - 3506.

Martin, A.K., Goodlad, S.W., Hartnady, C.J.H., and du Plessis, A., 1982. Cretaceous paleopositions of the Falkland Plateau relative to southern Africa using Mesozoic seafloor spreading anomalies. Geophys. J. R. astr. Soc., 71: 567-579.

Matthews, D.J., 1939. Tables of the velocity of sound in pure water and sea water for use in echo-sounding and sound-ranging. Hydrogr. Dep., The Admiralty, London, 1939.

McKenzie, D.P., 1967. Some remarks on heat flow and gravity anomalies. J. Geophys. Res., 72: 6261 - 6273.

McKenzie, D.P., Watts, A., Parsons, B., Roufosse, M., 1980. Planform of mantle convection beneath the Pacific Ocean. Nature, 288: 442 - 446.

Menard, H. W., 1973. Depth anomalies and the bobbing motion of drifting islands. J. Geophys. Res., 78: 5128 - 5137.

Müller, R.D. and Scotese, C.R., 1987. The tectonic development of the North Atlantic: Revised seafloor spreading isochrons and tectonic fabric map from Seasat altimetry. Inst. for Geophysics, Univ. of Texas at Austin, POMP Project Report No.26 - 1287, unpublished.

Nürnberg, D., Müller, R.D., and Sclater, J.G., in prep. The tectonic history of the South Atlantic from Jurassic to present.

Nürnberg, D., Müller, R.D., and Scotese, C.R., 1987. The fit of the continents around the South Atlantic. Paleoceanographic Mapping Project Progress Report No.22 - 0787, unpublished.

Parker, R.L and Oldenburg, D.W., 1973. Thermal model of ocean ridges. Nature Phys. Sci., 242: 137 - 139.

Pardo-Casas, F. and Molnar, P., 1987. Relative motion of the Nazca (Farallon) and South American plates since Late Cretaceous time. Tectonics, 6(3): 233 - 248.

Parsons, B. and Daly, S., 1983. The relationship between surface topography, gravity anomalies, and temperature structure of convection. J. Geophys. Res., 88: 1129 - 1144.

Parsons and Freedman, 1987

Parsons, B. and McKenzie, D.P., 1978. Mantle convection and the thermal structure of the plates. J. Geophys. Res., 83: 4485 - 4496.

Parsons, B. and Sclater, J.G., 1977. An analysis of the variation of ocean floor bathymetry and heat flow with age. Jour. Geophys. Res., Vol. 82(5)

Pitman III, W.C.and Talwani, M., 1972. Seafloor spreading in the North Atlantic. Geol. Soc. Amer. Bull., 83: 619 - 646.

Rabinowitz, P.D., and LaBrecque, J., 1979. The Mesozoic South Atlantic Ocean and evolution of its continental margins. Journal of Geophys. Research, 84(B11): 5973-6002.

Renkin, M. and Sclater, J.G., 1988. Depth and Age in the North Pacific. Jour. Geophys. Res., 93(B4): 2919 - 2935.

Renkin, M., 1986. Age,depth and residual depth anomalies in the North Pacific: Implications for thermal models of the lithosphere and upper mantle. M.A. thesis, 117 pp., Univ. of Texas at Austin, Austin, 1986.

Ross, M.I. and Scotese, C.R., in prep. Hierarchical Tectonic Analysis of the Gulf of Mexico and Caribbean Region.

Sandwell, D.T., 1984. Along-track deflection of the vertical from Seasat: GEBCO overlays. NOAA Technical Memorandum NOS NGS-40.

Sandwell, D.T. and Renkin, M., 1988. Compensation of swells and plateaus in the North Pacific: no direct evidence for mantle convection. J. Geophys. Res., 93(B4): 2775 -2783.

Sandwell, D.T. and McKenzie, in prep.

Sclater, J.G., Jaupart, C., and Galson, D., 1971. The heat flow through oceanic and continental crust and the heat loss of the earth. Rev. Geophys., 18: 269 - 311.

Sclater, J.G. and McKenzie, D.P., 1973. Paleobathymetry of the South Atlantic. Geol. Soc. Amer. Bull., 84: 3203 - 3216.

Sclater, J.G., Meinke, L., Bennett, A., and Murphy, C., 1985. The depth of the ocean through the Neogene. Geol. Soc. Amer. Memoir, 163, 1985.

Sclater, J.G. and Wixon, L., 1986. The relationship between depth and age and heat flow and age in the western North Atlantic. in The western Atlantic region, Vol. M,

Geology of North America, edited by P.R. Vogt and B.E. Tucholke, pp. 257 - 270, Geological Society of America, Boulder, Col..

Schroeder, W., 1984. The empirical age-depth relation and depth anomalies in the Pacific Ocean basin. J. Geophys. Res., 89(B12): 9873 -9883.

Turcotte, D.L. and Oxburgh, E.R., 1967. Finite amplitude convection cells and continental drift. J. Fluid. Mech., 28: 29 - 42.

Watts, A.B. and Daly, S.F., 1981. Long wavelength gravity and topography anomalies. Annual Rev. Earth Planet. Sci., 9: 415 - 448.

Watts, A.B. and Ribe, N.M., 1984. On geoid heights and flexure of the lithosphere at seamounts. J. Geophys. Res., 89: 11152 - 11170.

Watts, A.B., McKenzie, D.P., Parsons, B., and Roufosse, M., 1985. The relationship between gravity and bathymetry in the Pacific Ocean. Geophys. J. R. astro. Soc., 83: 263 - 298.

Figures

Figure 1: (a) Schematic diagram showing the one-layer simple cooling, square root of age model. The distance from ridge crest is roughly equivalent to age. The lithosphere increases in thickness with age. Thereby, the bottom boundary is an isotherm. Continuous lines are isotherms, and Ts is the temperature of the asthenosphere. (Bottom) The interaction between the simple cooling model and a mid-plate "hot spot" is shown. Between the ridge crest and the hot spot, the lithosphere thickens and subsides by cooling. The hot spot causes thinning of the lithosphere and uplift by adding extra heat from below. (b) Schematic diagram showing the two-layer, thermo-mechanical, "plate" model. The oceanic lithosphere is divided into a rigid mechanical layer and a viscous thermal boundary layer. Instability in the viscous thermal boundary layer causes both layers to flatten under old ocean floor. The temperature structure of both layers, when in equilibrium, is shown on the right. (Bottom) The interaction between isotherms in an upper mantle convection plume and the thermo-mechanical model is shown. The effect of the convection plume-center on the thermal structures of the lithosphere is exhibited by the dashed line on the right. Diagrams are taken from Renkin and Sclater (1988).

Figure 2: Tectonic map for the South Atlantic showing magnetic anomaly data and fracture zones. Magnetic anomaly picks and lineations are taken from Cande et al. (in press), Rabinowitz and LaBrecque (1979), LaBrecque and Hayes (1979), Barker (1979) and Martin et al. (1982). The locations of fracture zones are derived from Seasat geoid height and marine geophysical data (Cande et al., in press). The location of the ridge axis is based on a combination of magnetic and topographic profile and GEBCO (Cande et al., in press).

Figure 3: Isochron chart of the South Atlantic based on the magnetic anomaly data compilation of Cande et al. (in press), Rabinowitz and LaBrecque (1979), LaBrecque and Hayes (1979), Barker (1979) and Martin et al. (1982). The tectonic history of the South Atlantic opening from late Jurassic to present day is outlined in Nürnberg et al. (in prep.).

Figure 4: Bathymetric chart of the South Atlantic from the ETOPO5 world topographic and bathymetric database (NOAA). These data were averaged in half by half degree intervals. The depths are corrected for the variations of the velocity of sound in seawater according to Matthews (1939) and contoured in 500 m intervals.

Figure 5: Sediment thickness map of the South Atlantic from Divins and Rabinowitz (in press). DSDP- sites that reached basement (solid circles) or ended in sediments (open circles), respectively, are superimposed. Sediment thickness in meters.

Figure 6: Sediment thickness map of the South Atlantic in two-way travel reflection time [sec] (after Divins and Rabinowitz, in press).

Figure 7: Diagram showing the relationship between two-way travel reflection time of seismic waves through the sediment column and the standard mass balance sediment correction for 10 DSDP sites in the South Atlantic. The linearity of this relationship, which is due to the self-cancellation of increases in velocity and density with depth, indicates that the Crough-correction for sediment loading (Crough, 1983) holds for the South Atlantic.

Figure 8: The depth versus age for the South Atlantic for all ages using all data. Figure 8a shows the actual data set. Each point plotted represents the value determined for each single half by half degree element. A histogram of the number of points in each 1-Ma age band is shown above the plot of depth versus age. In Figure 8b the mean solid line) and the upper and lower standard deviations about the mean (dashed lines) are computed at 1-Ma intervals with the points weighed for the decrease in area of the half degree elements with increasing latitude. Figure 8c exhibits contours enclosing approximately two-thirds of the points around the mode. The number of points that fell in each 1-Ma x 100 m square was stored, and the resulting grid was contoured. Before being contoured, the point counts were weighed for the decrease in area of a half by half degree element with increasing latitude The dashed and solid smooth curves superimposed on each diagram reflect the relations expected from the two-layer thermo-mechanical, plate model and the single-layer, square root of age model (Parsons and Sclater, 1977), respectively.

Figure 9: Histograms taken at 20-Ma intervals along the depth versus age distribution for the South Atlantic. The distribution of depths with age exhibits a significant scatter at all ages. However, it increases on crust older than 80 Ma.

Figure 10: The depth versus age for the South Atlantic. Plotted are all data except data for the Rio Grande Rise and Walvis Ridge, defined by the 4000m isobath. The histogram and curves in Figures 10b and 10c are explained in Figure 8.

Figure 11: The depth versus age for the eastern part of the South Atlantic. The histogram and curves in Figures 12b and 12c are explained in Figure 8.

Figure 12: The depth versus age for the western part of the South Atlantic. The histogram and curves in Figures 11b and 11c are explained in Figure 8.

Figure 13: The depth versus age for the Argentine Basin. The histogram curves in Figures 13b and 13c are explained in Figure 8.

Figure 14: The depth versus age showing the actual data set for each 5-degree strip of latitude over the entire width of the South Atlantic. The data set is divided according to the African plate (open squares) and South American plate (crosses). Superimposed on each plot are the curves reflecting the relations expected from the two-layer thermo-mechanical, plate model (dashed line) and the single-layer, square root of age model (solid line) (Parsons and Sclater, 1977), respectively.

Figure 15: Mean (solid line), upper and lower standard deviation (dashed lines) corresponding to the depth versus age plots from Figure 14 for the western flank (South American plate) of the South Atlantic.

Figure 16: Mean (solid line), upper and lower standard deviation (dashed lines) corresponding to the depth versus age plots from Figure 14 for the eastern flank (African plate) of the South Atlantic.

Figure 17: Contours enclosing approximately two-thirds of the points around the mode for each 5-degree strip of oceanic crust separated by South American and African plate.

Figure 18: Residual depth anomalies in the South Atlantic, averaged for half by half degree elements. Contours are in meters. The largest anomalies appear at the Rio Grande Rise, the Walvis Ridge and the Abrolhos Plateau off Brazil.

Figure 19: Residual depth anomalies in the South Atlantic, smoothed by using a low-pass Gaussian filter, which removes wavelengths shorter than 600 km.

Figure 20: Smoothed geoid for the South Atlantic Ocean. Wavelengths greater than 4000 km are removed from the Seasat and GEOS 3 satellite altimeter data of Marsh et al. (1986).

BOUNDARY LAYER MODELS OF OCEANIC LITHOSPHERE

a. SIMPLE COOLING '$\sqrt{t}$'

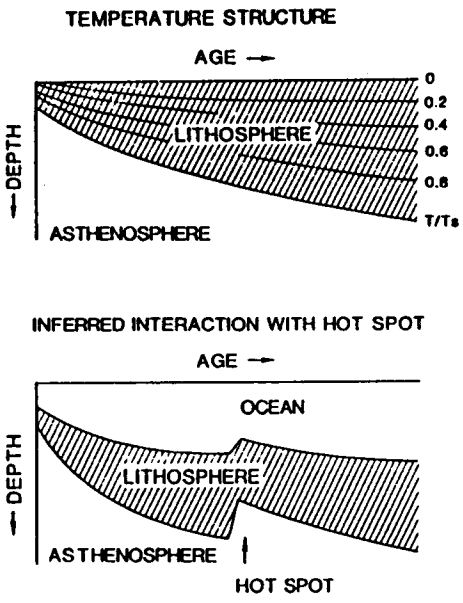

b. THERMO-MECHANICAL ' PLATE '

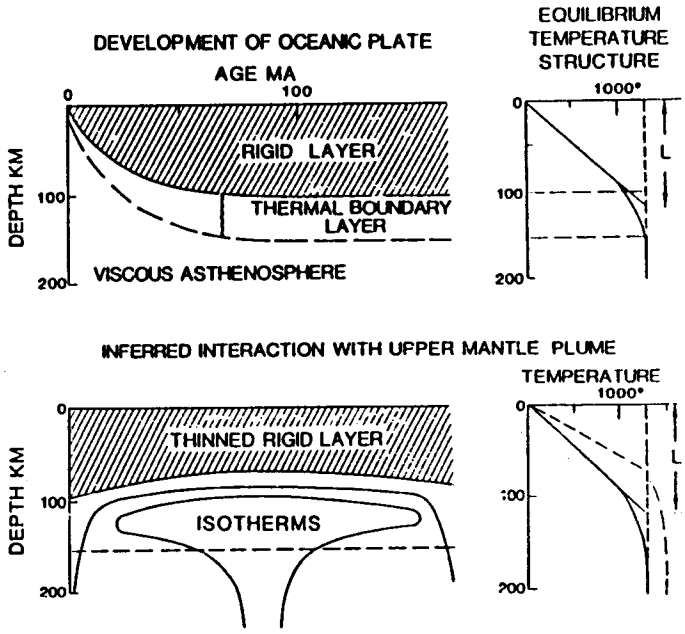

Fig. 1

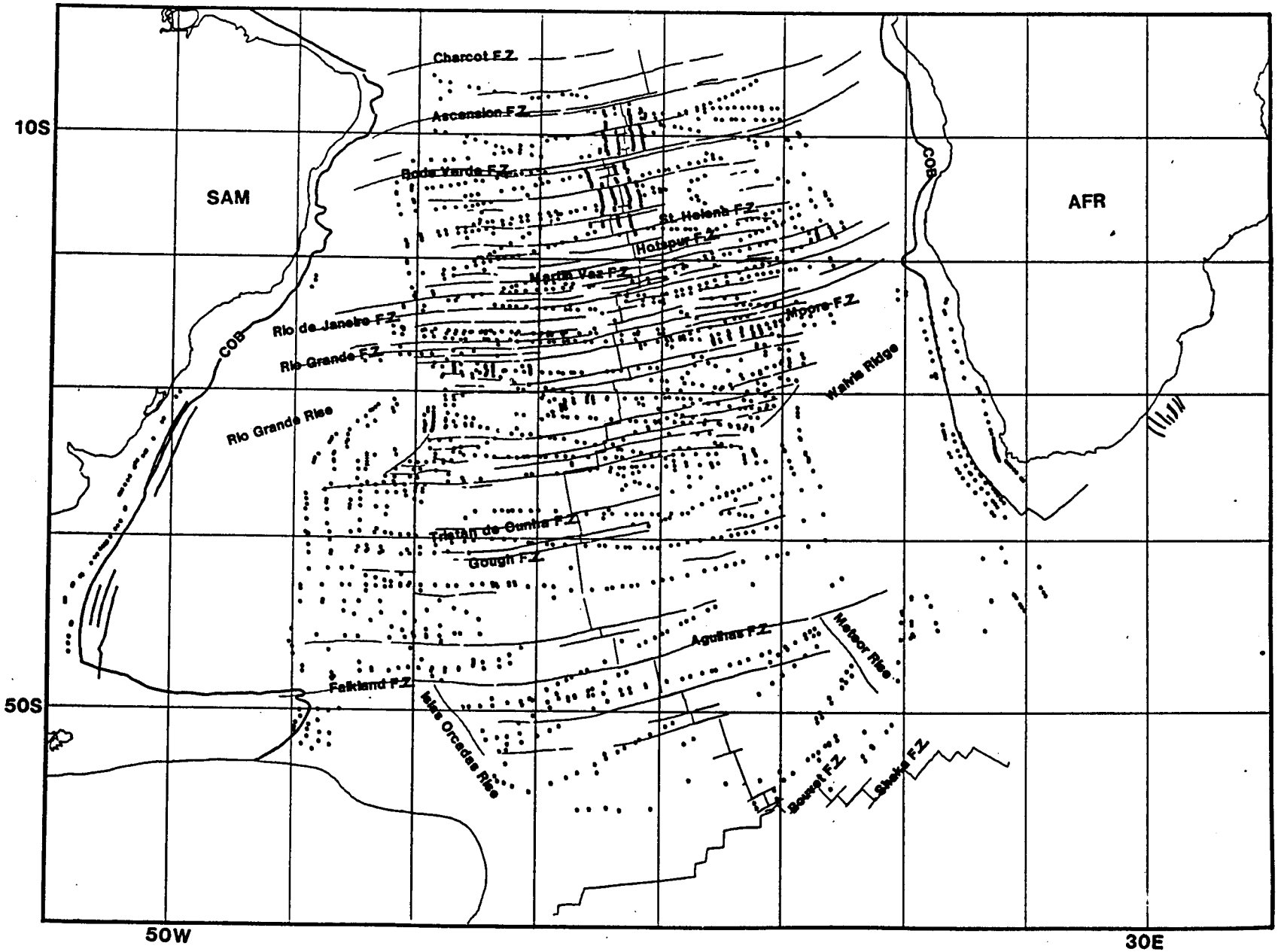
Charcot F.Z.
Ascension F.Z.
Bode Verde F.Z.
St. Helena F.Z.
Hotspur F.Z.
Maria Vas F.Z.
Mppre F.Z.
Rio de Janeiro F.Z.
Rio Grande F.Z.
Rio Grande Rise
Walvis Ridge
Tristan da Cunha F.Z.
Gough F.Z.
Agulhas F.Z.
Meteor Rise
Falkland F.Z.
Ilsas Orcadas Rise
Bouvet F.Z.
Shaka F.Z.
COB
COB
SAM
AFR
10S
50S
50W
30E

Fig. 2

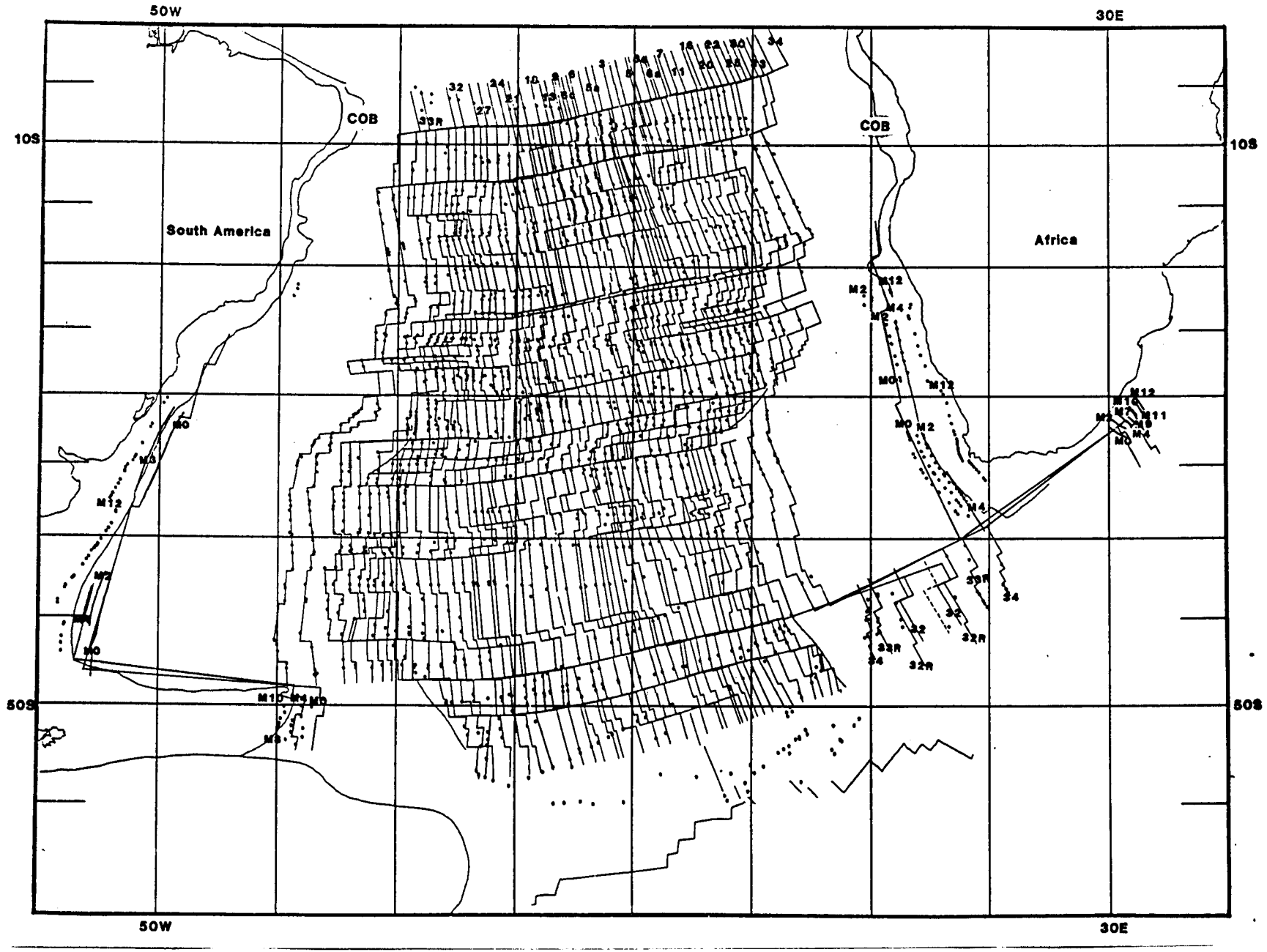

Fig. 3

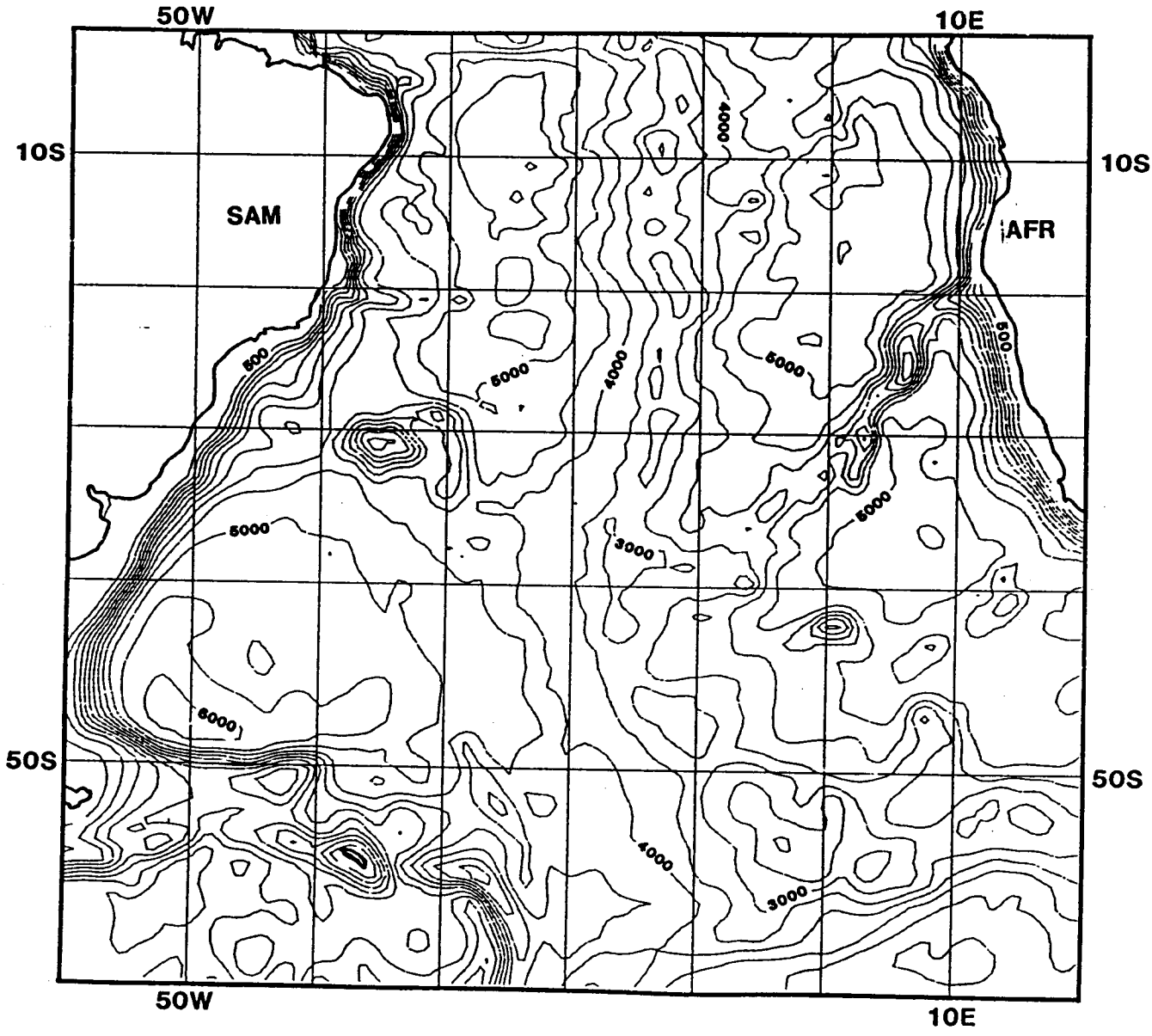

Fig. 4

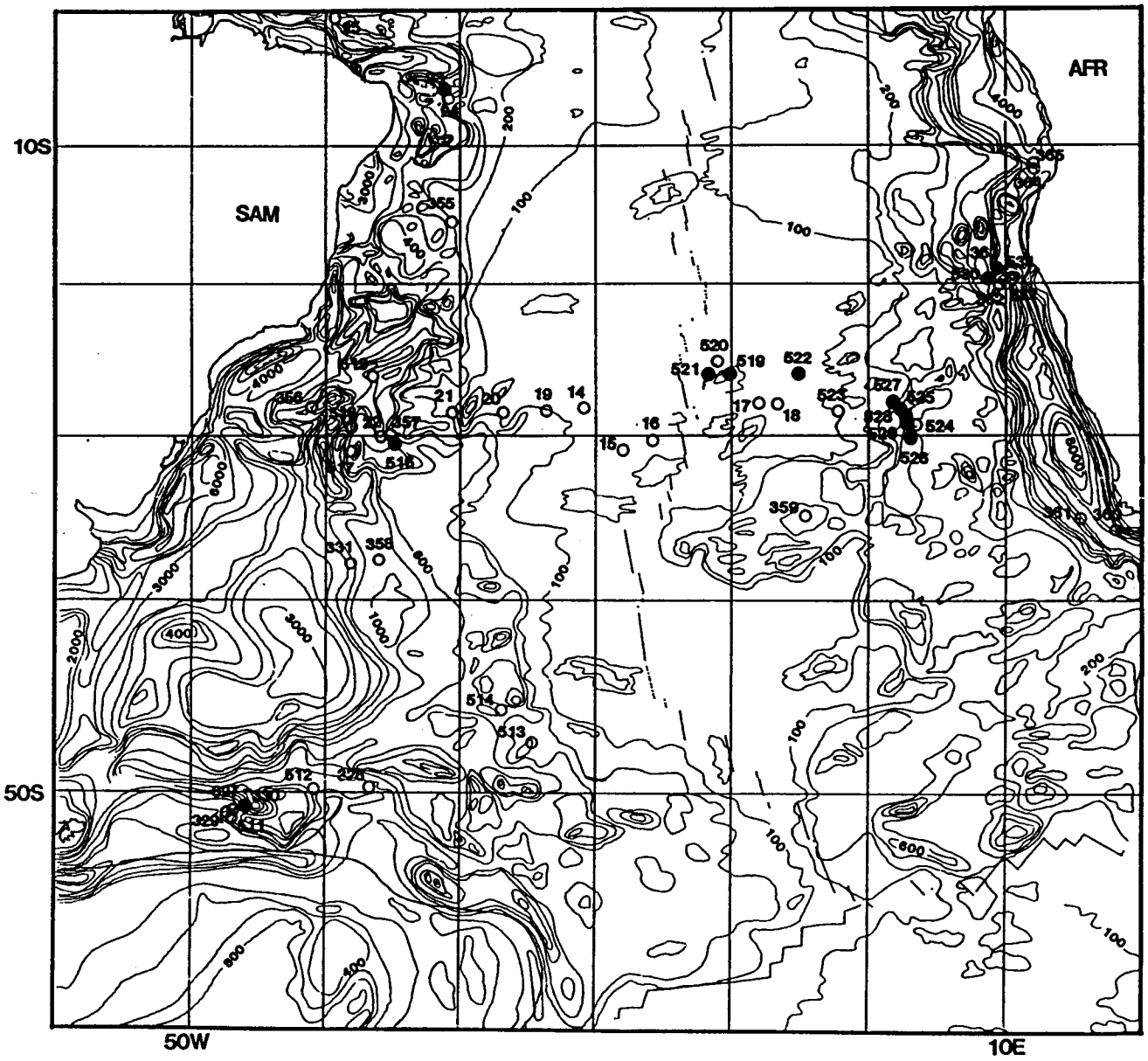
AFR
SAM
10S
50S
50W
10E
100
200
400
600
800
1000
2000
3000
4000
6000
8000
14
15
16
17
18
19
20
21
355
356
357
358
359
360
361
512
513
514
515
516
519
520
521
522
523
524
525
526
527
528

Fig. 5

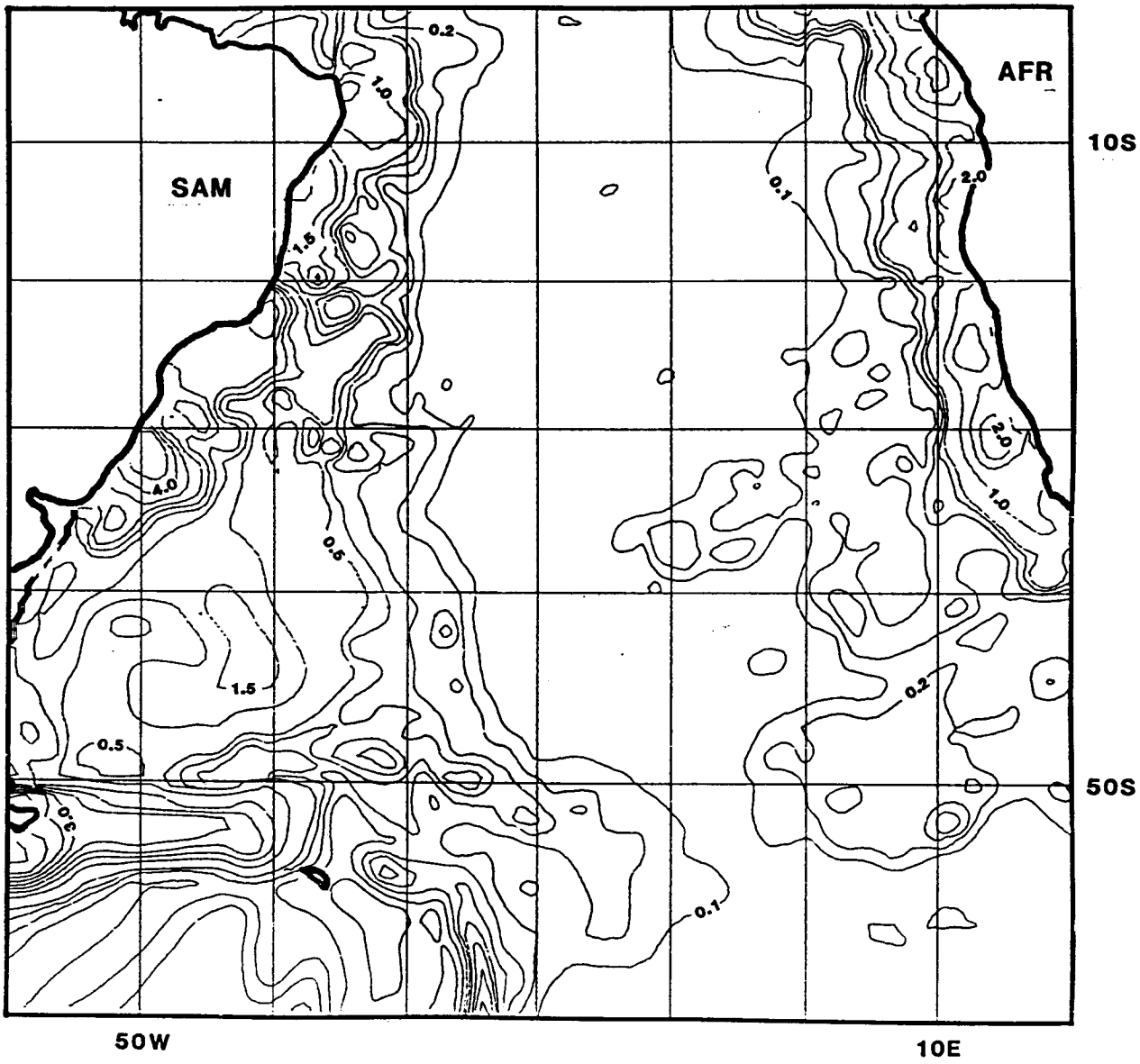

Fig. 6

CROUGH CORRECTION FOR SEDIMENT LOADING

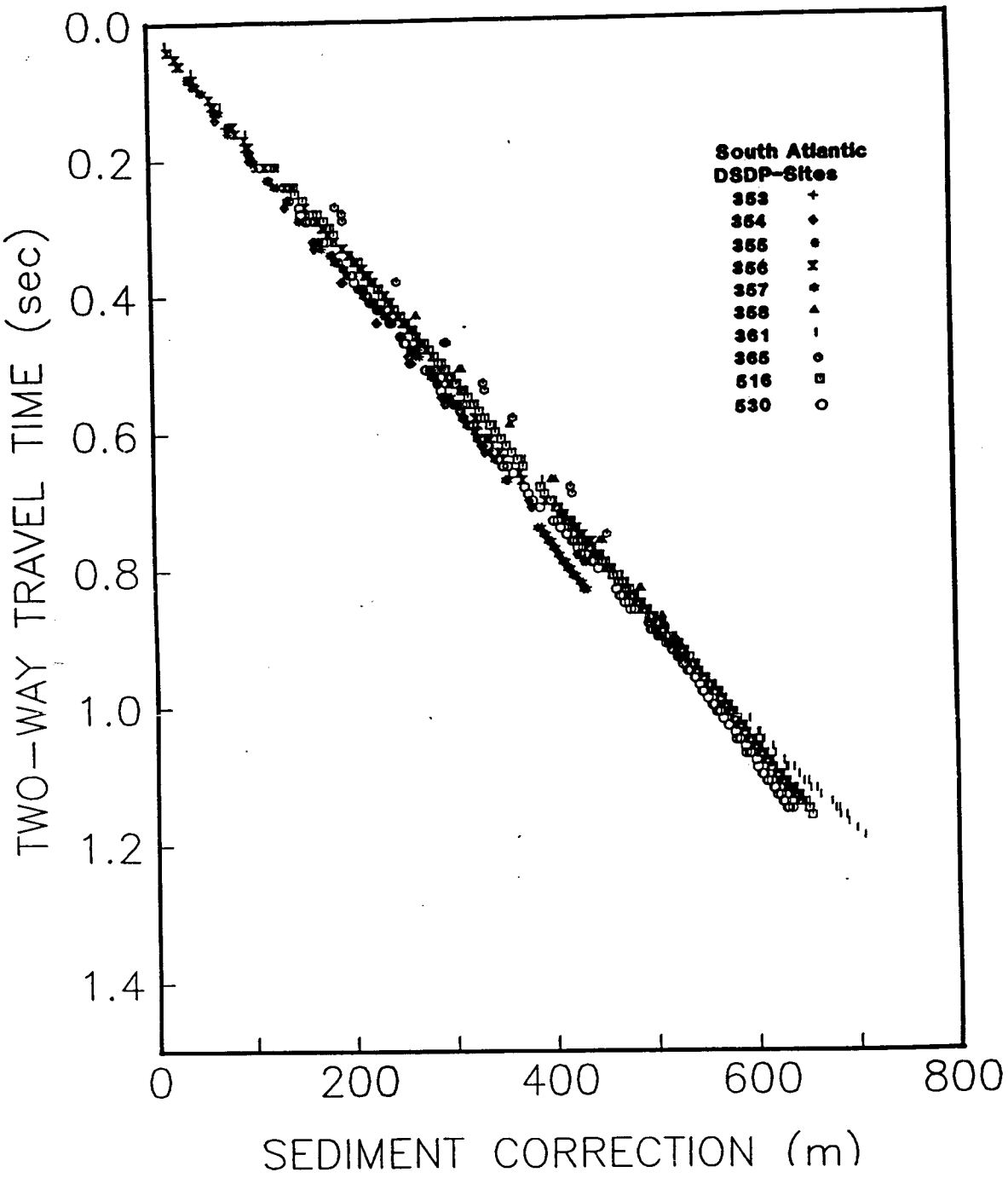

Fig. 7

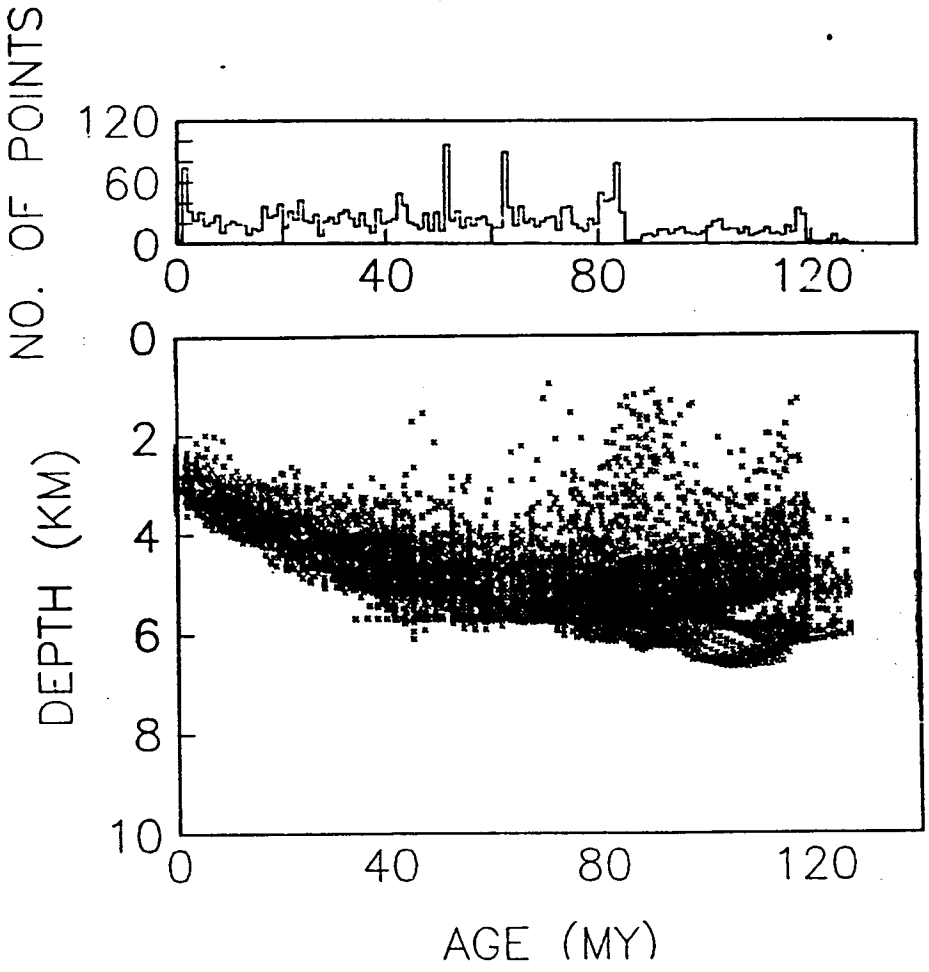
NO. OF POINTS
120
60
0
0
40
80
120
DEPTH (KM)
0
2
4
6
8
10
0
40
80
120
AGE (MY)

Fig. 8a

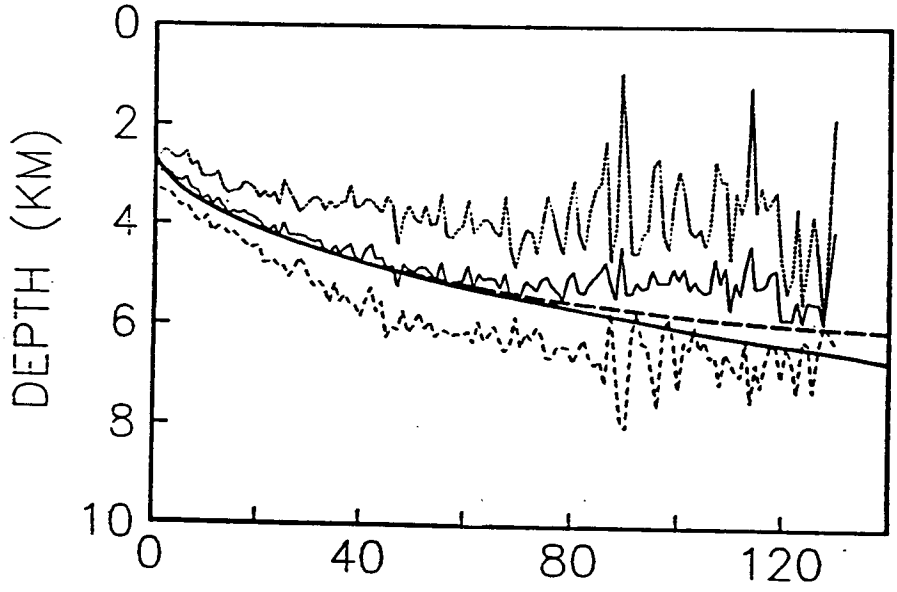

Fig. 8b

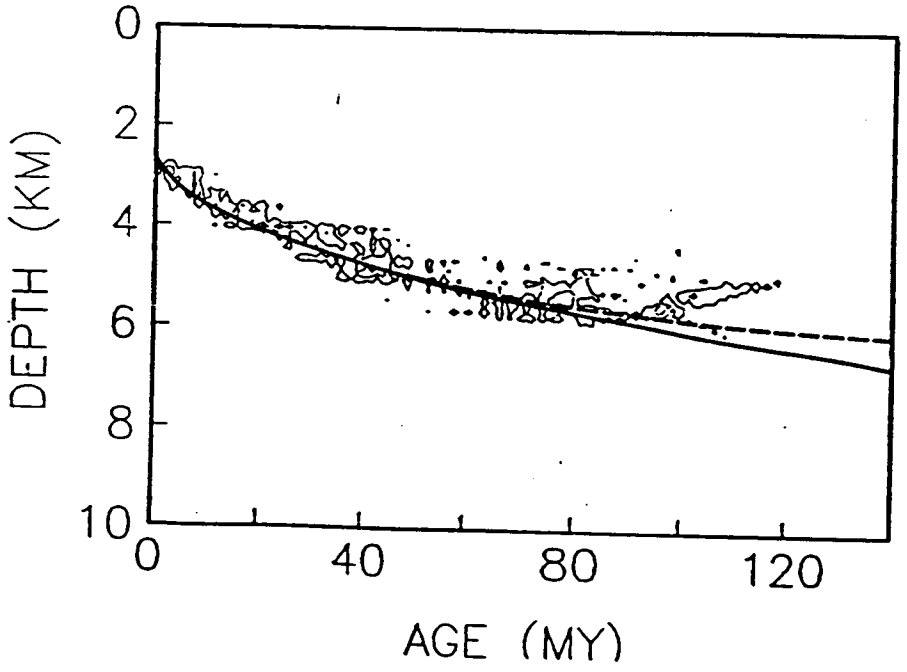

Fig. 8c

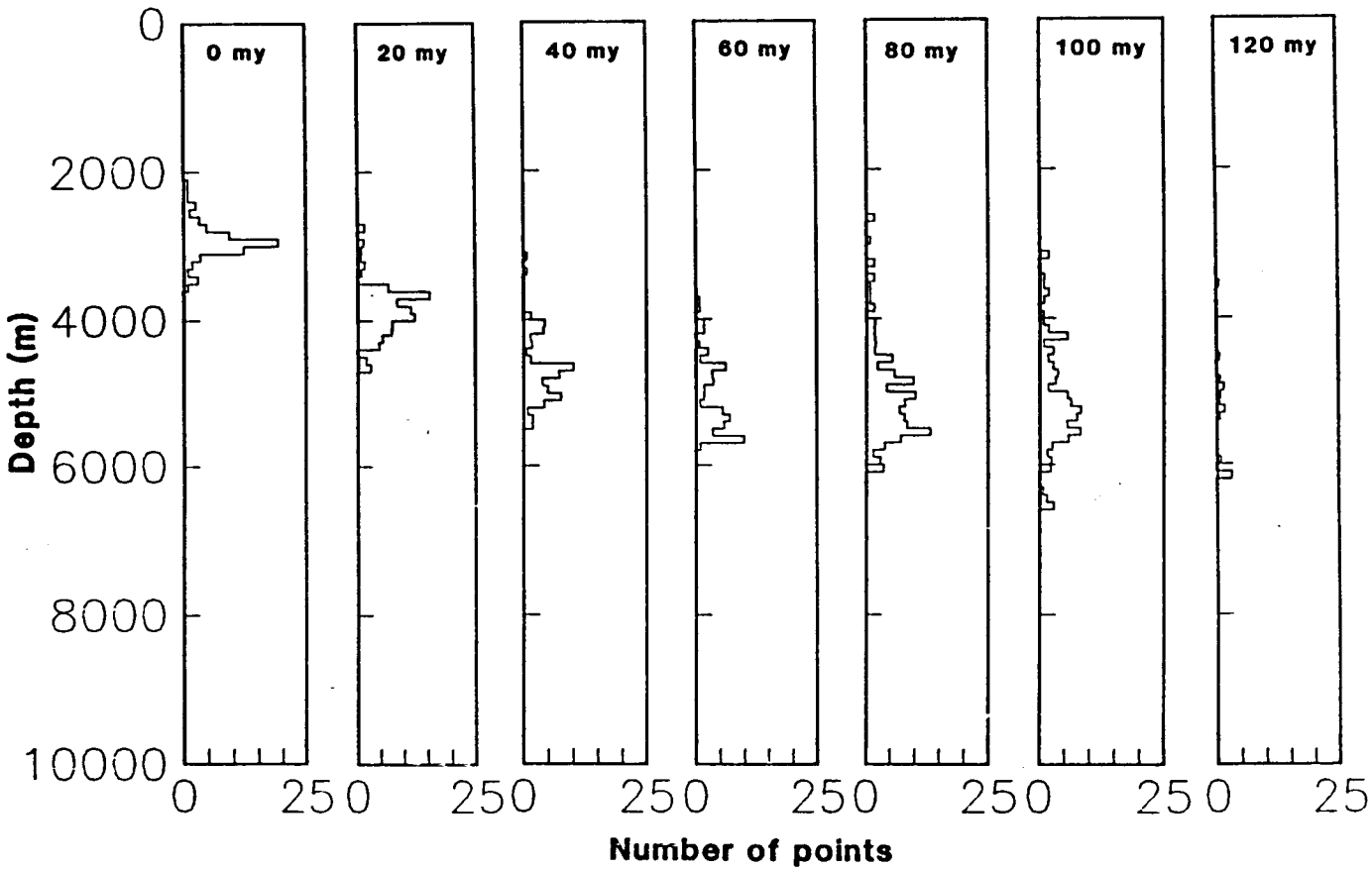
0 my
20 my
40 my
60 my
80 my
100 my
120 my
0
2000
4000
6000
8000
10000
Depth (m)
0
250
250
250
250
250
250
0
25
Number of points

Fig. 9

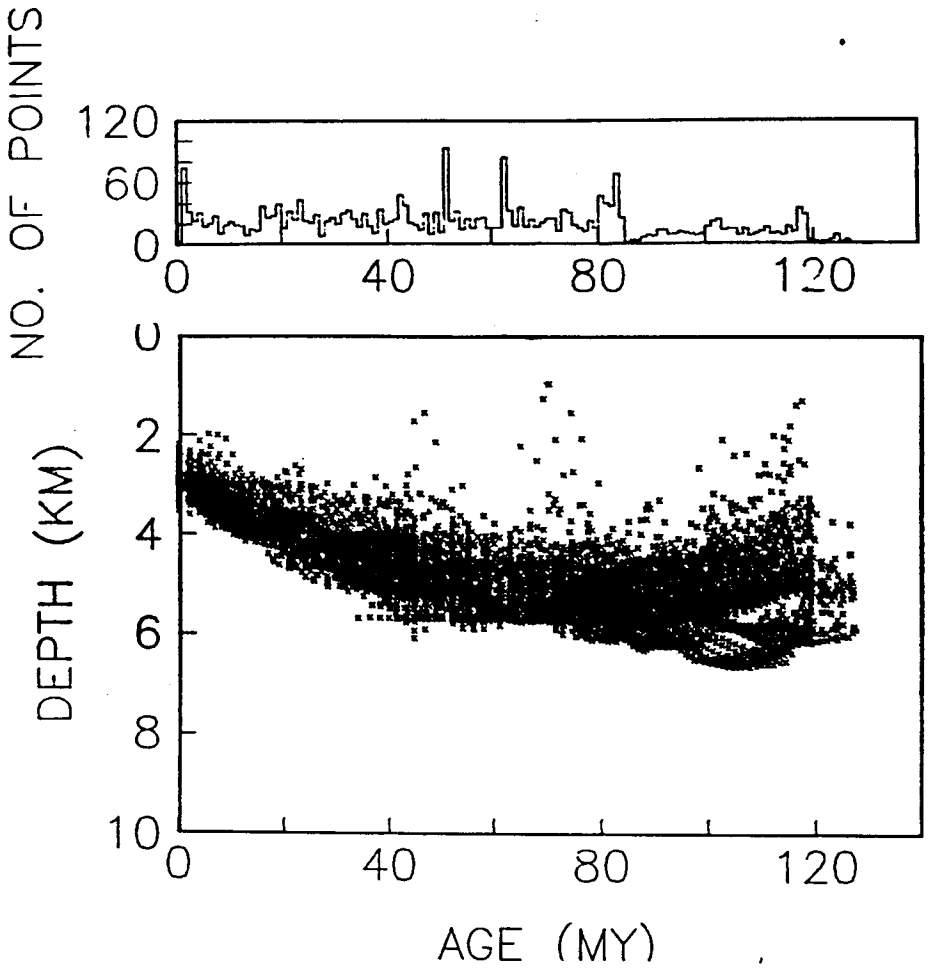
NO. OF POINTS
120
60
0
0
40
80
120
DEPTH (KM)
0
2
4
6
8
10
0
40
80
120
AGE (MY)

Fig. 10a

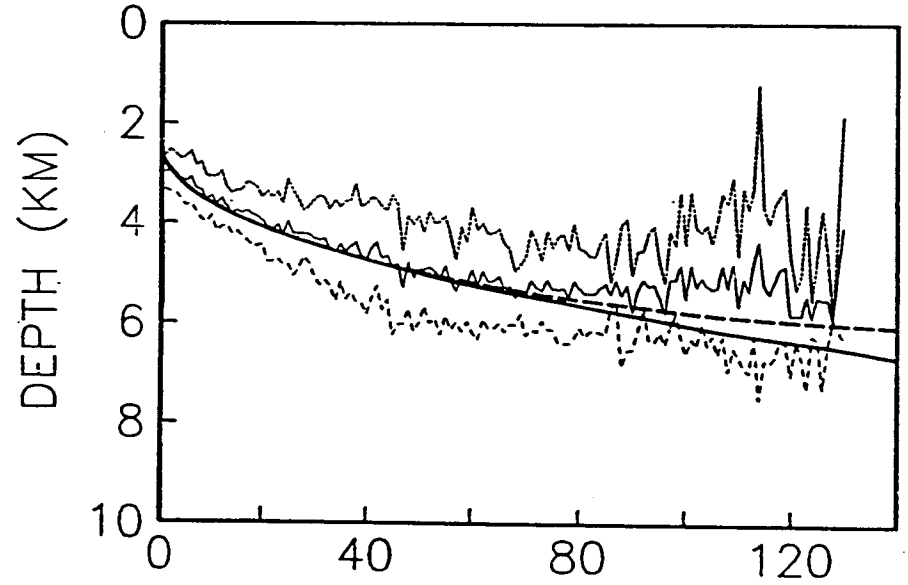

Fig. 10b

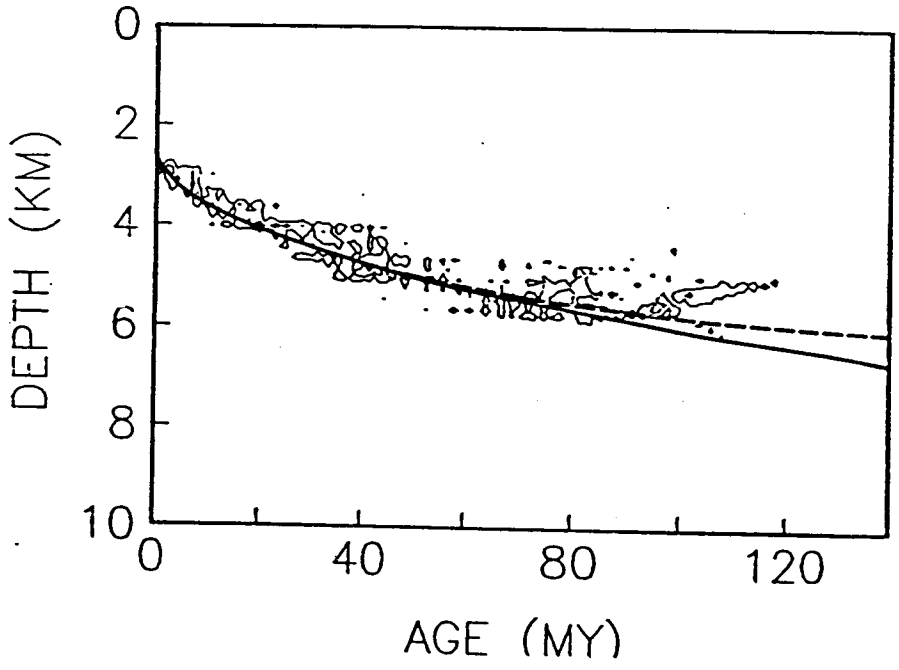

Fig. 10c

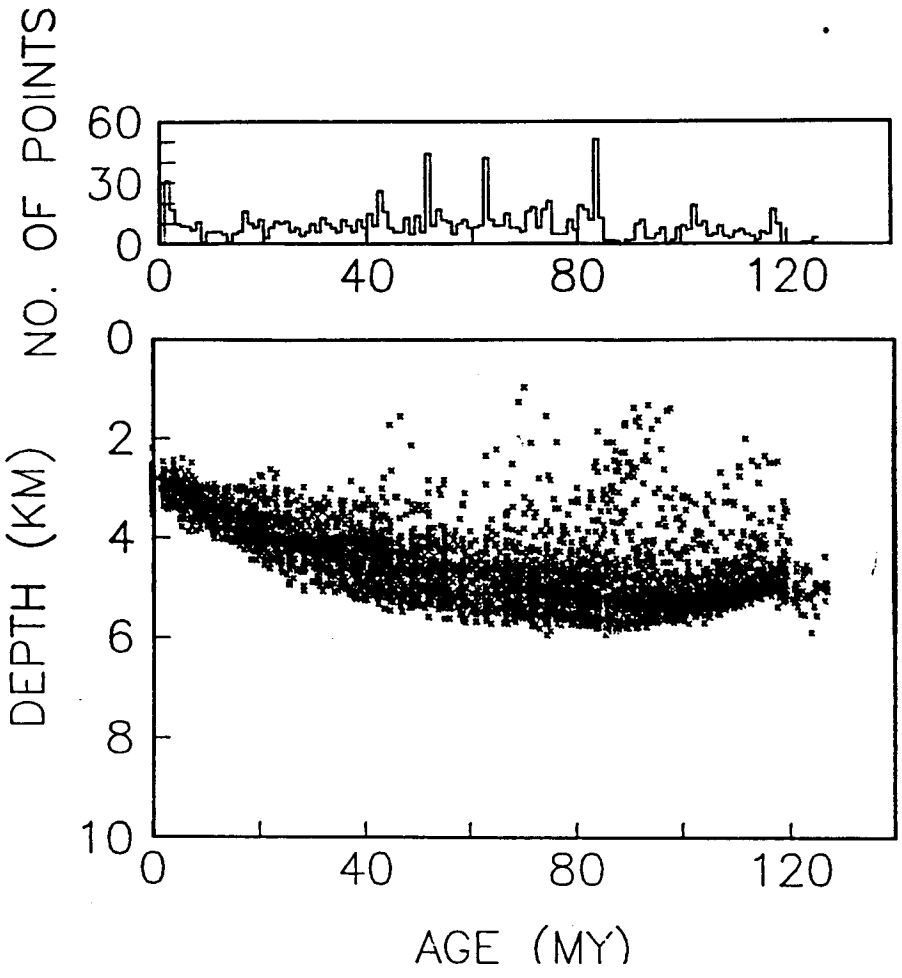
NO. OF POINTS
60
30
0
0
40
80
120
DEPTH (KM)
0
2
4
6
8
10
0
40
80
120
AGE (MY)

Fig. 11a

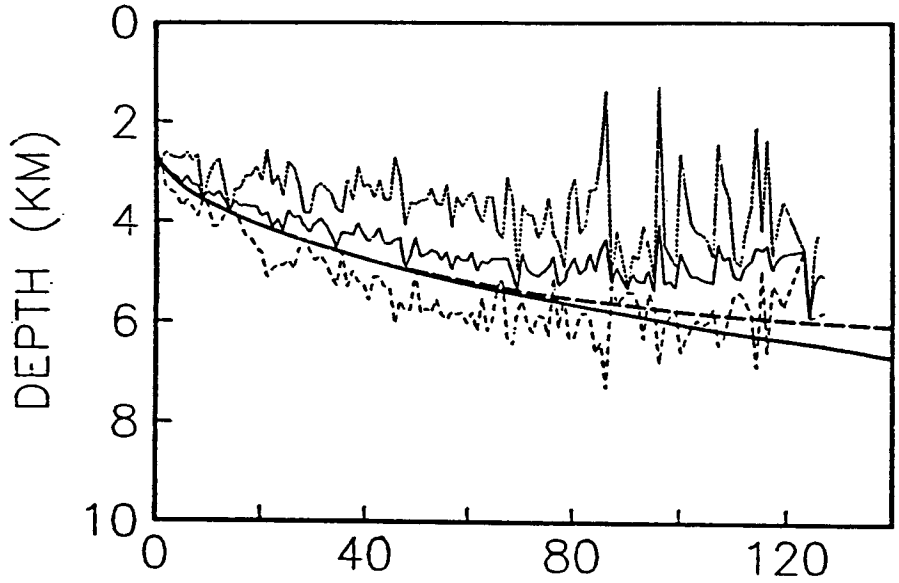

Fig. 11b

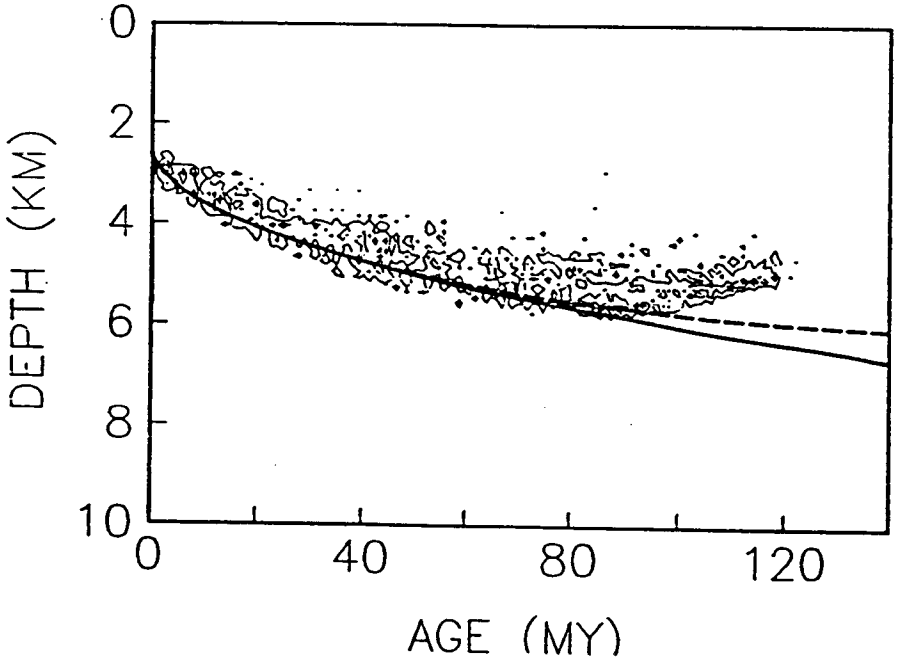

Fig. 11c

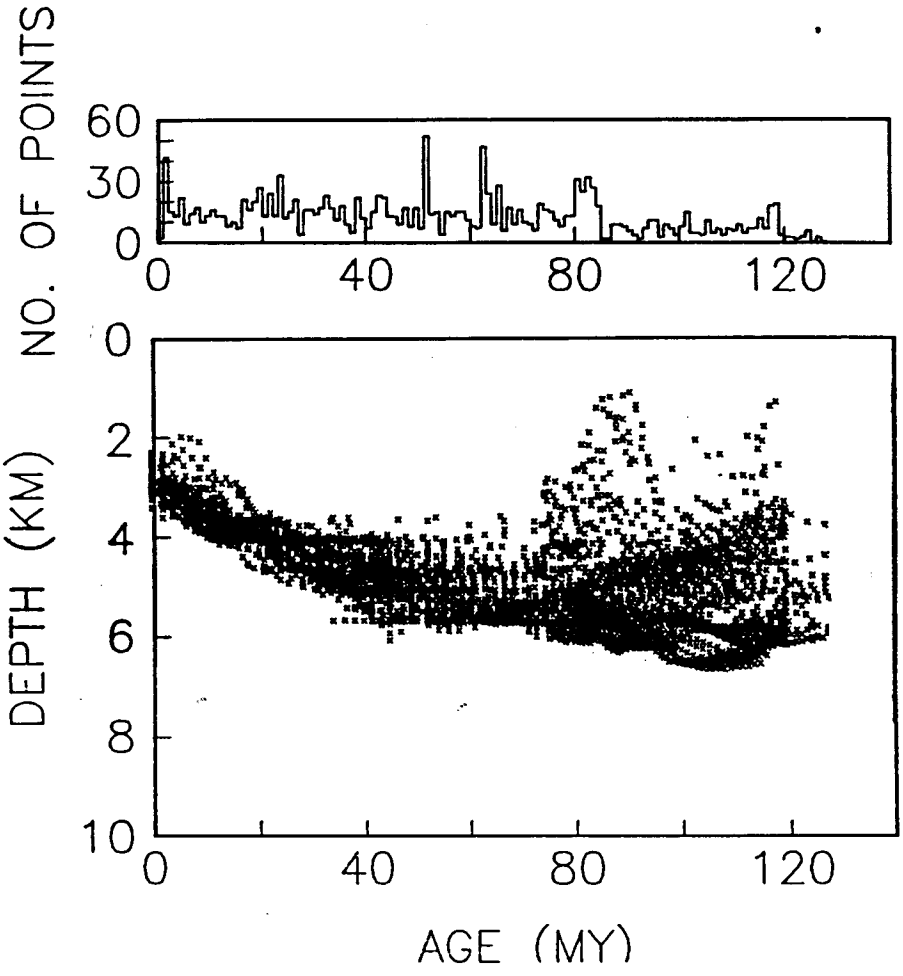
NO. OF POINTS
60
30
0
0
40
80
120
DEPTH (KM)
0
2
4
6
8
10
0
40
80
120
AGE (MY)

Fig. 12a

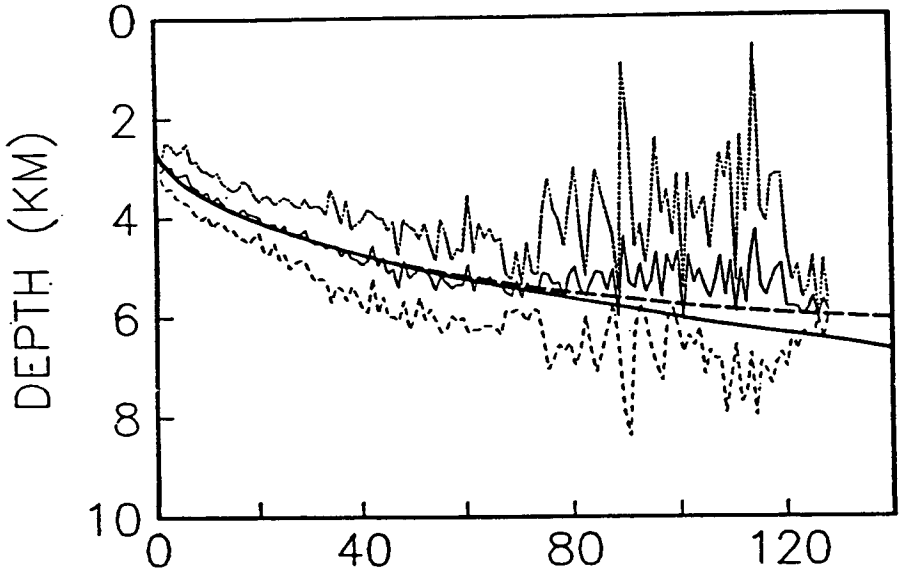

Fig. 12b

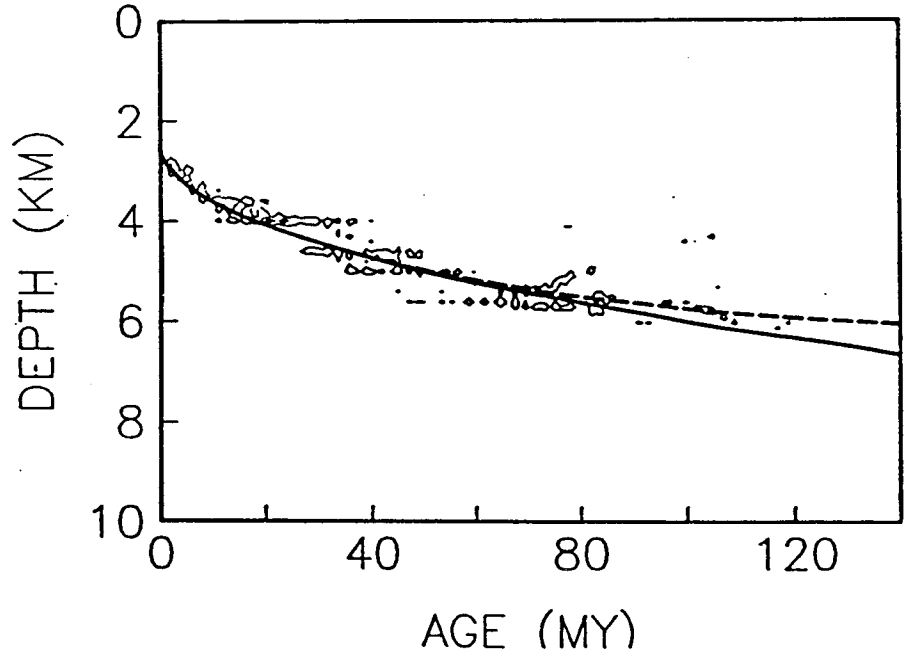

Fig. 12c

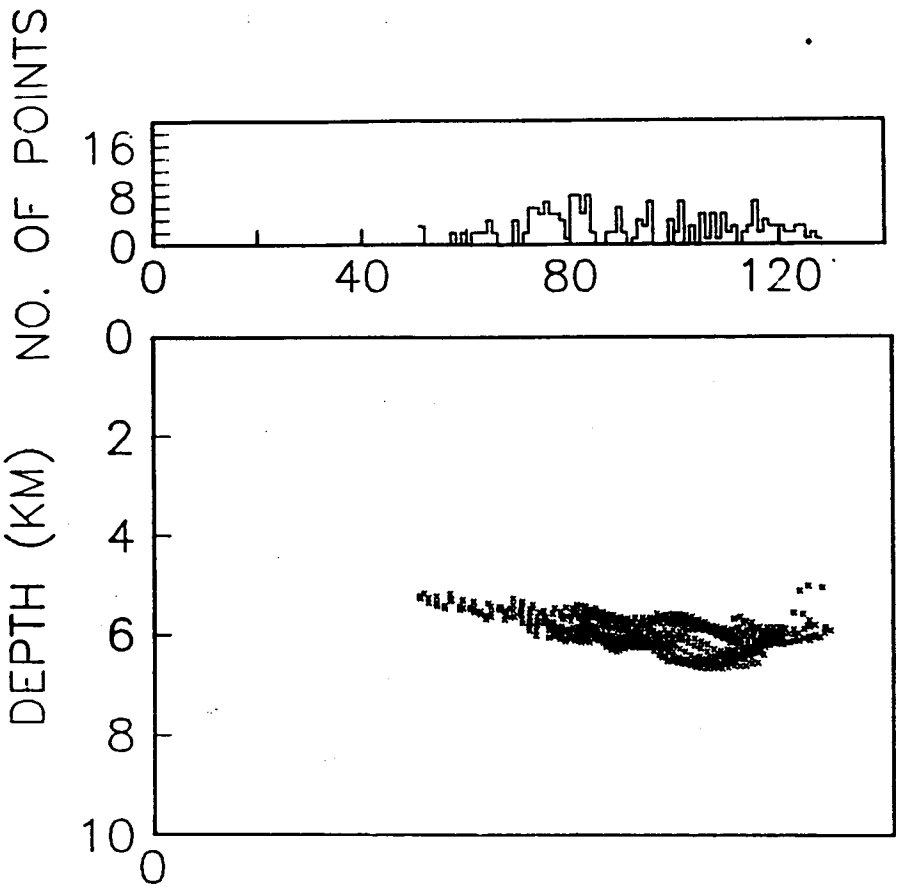

Fig. 13a

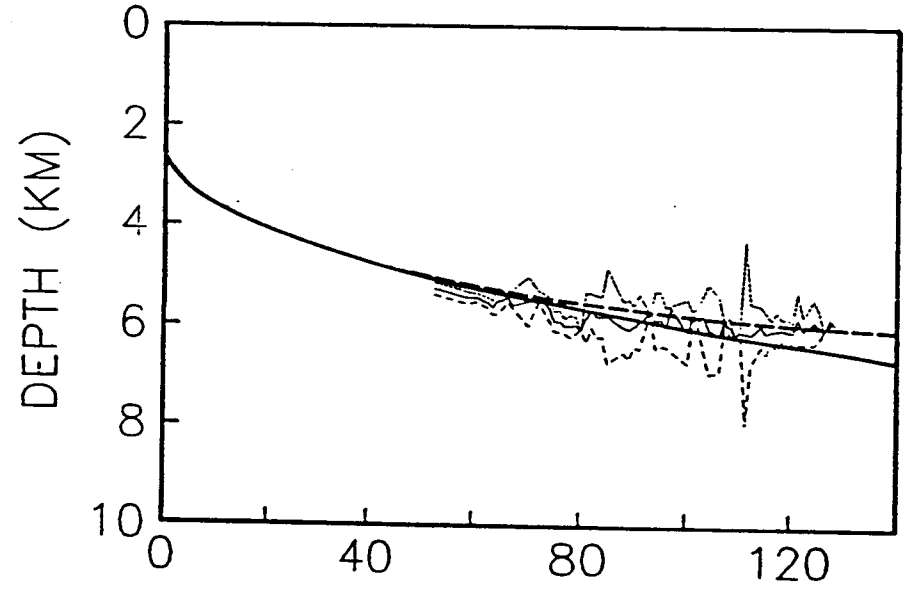

Fig. 13b

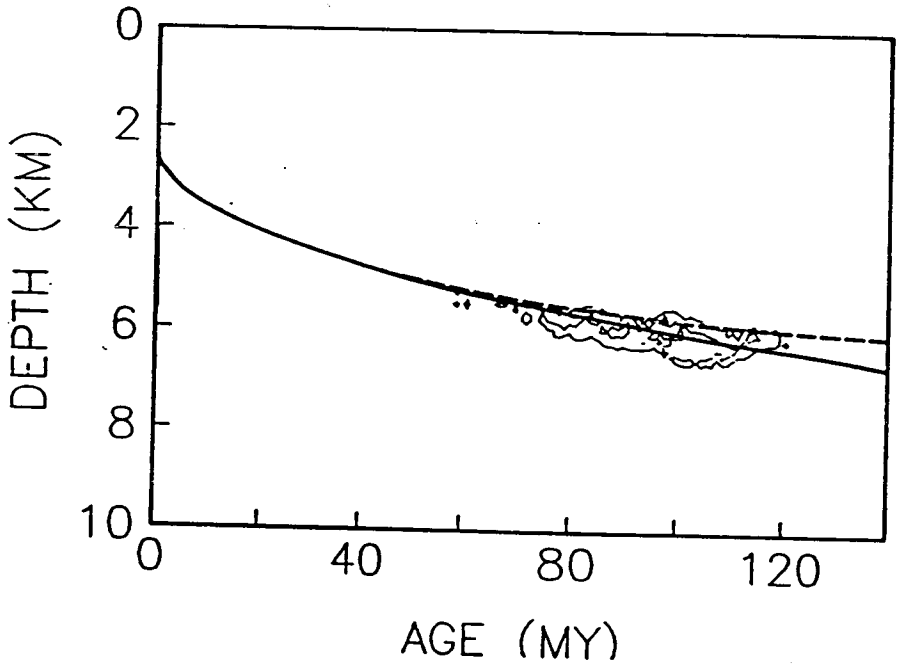

Fig. 13c

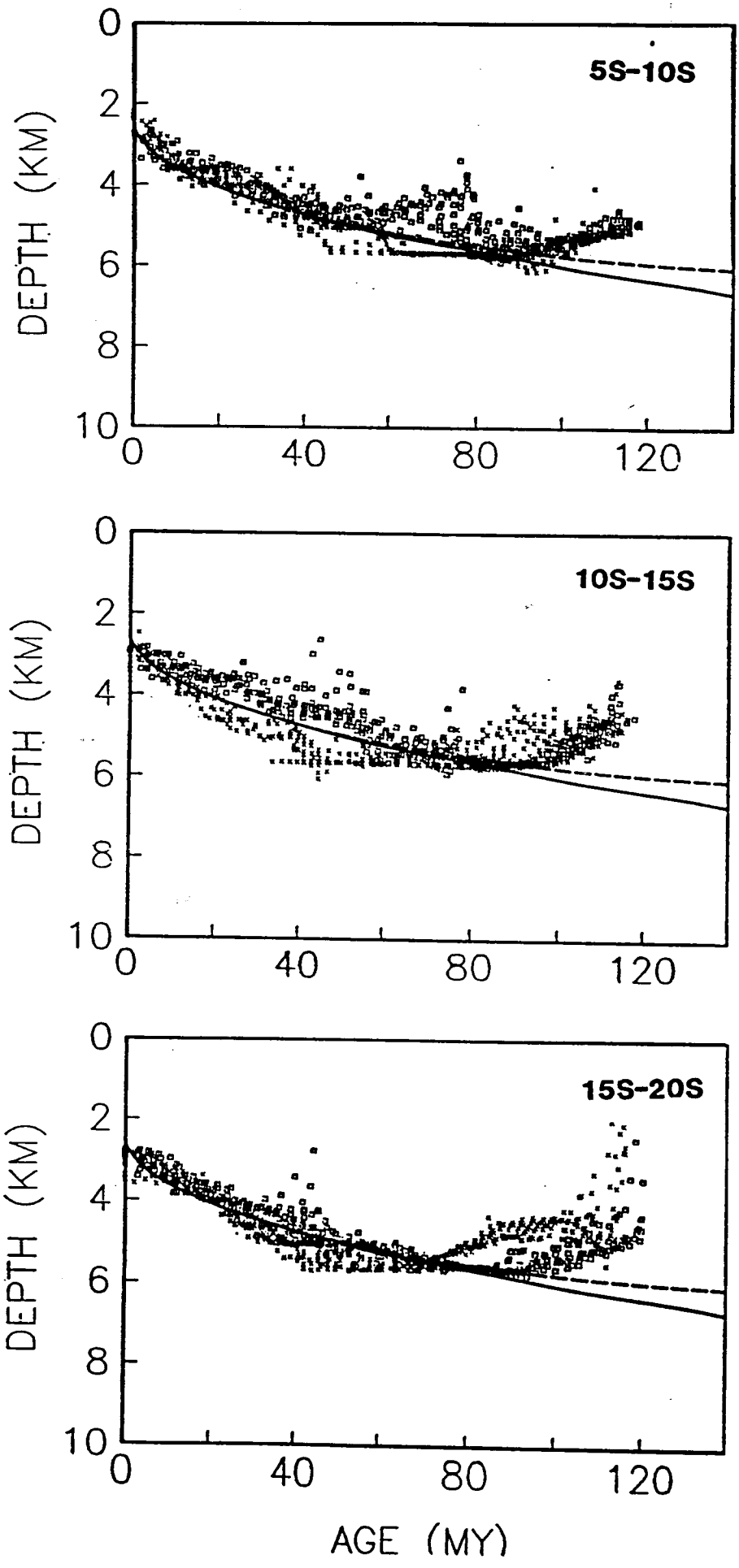

Fig. 14

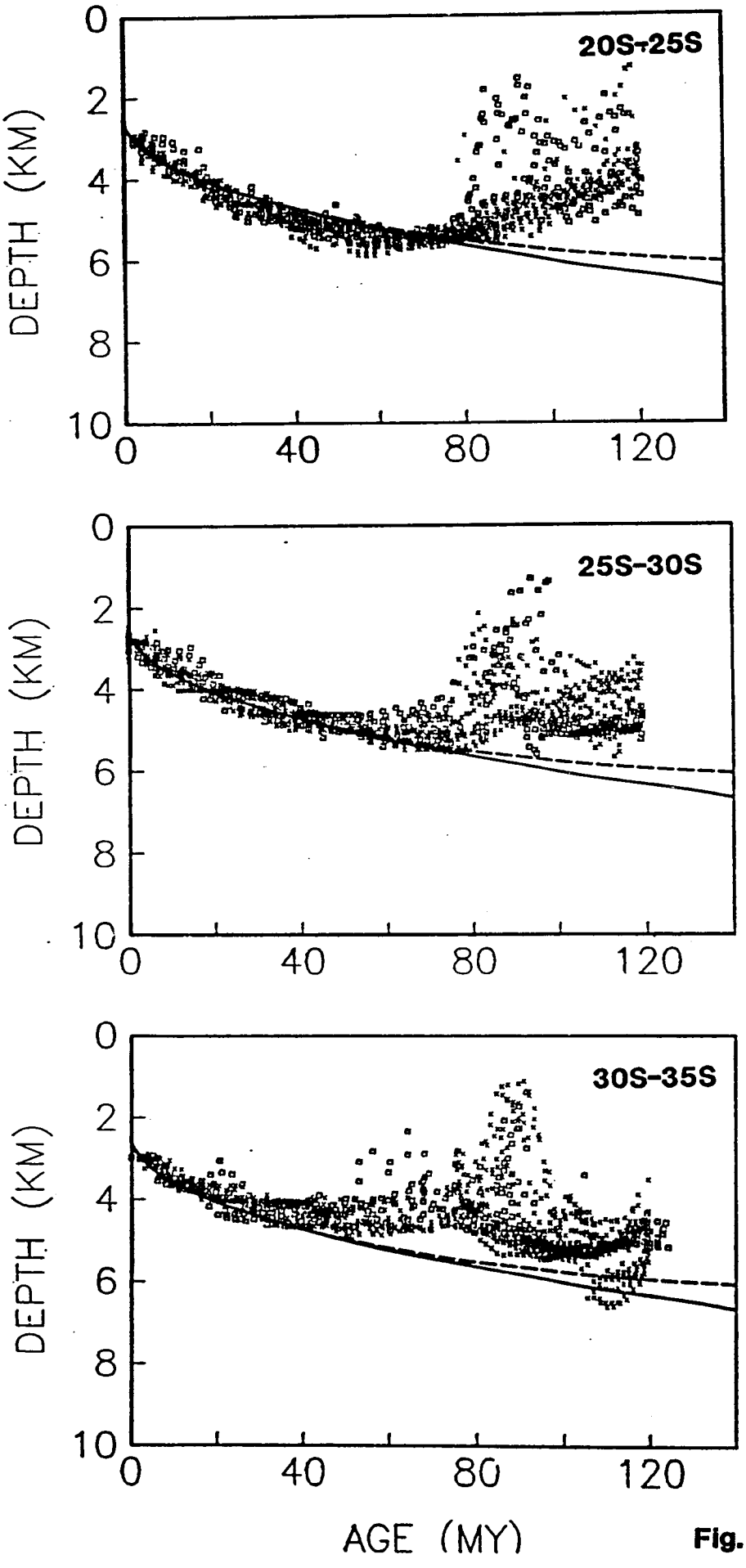

Fig. 14 continued

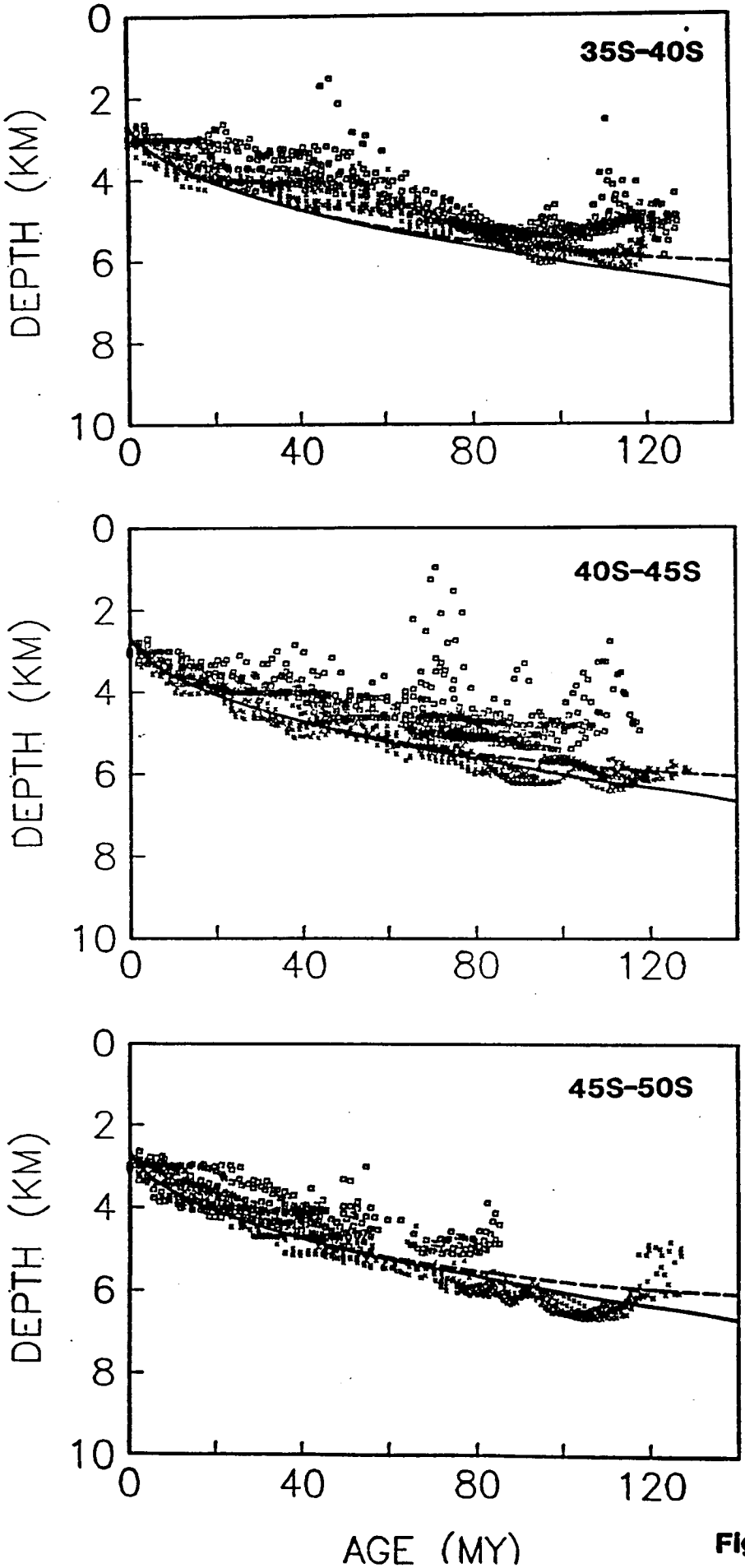

Fig. 14 continued

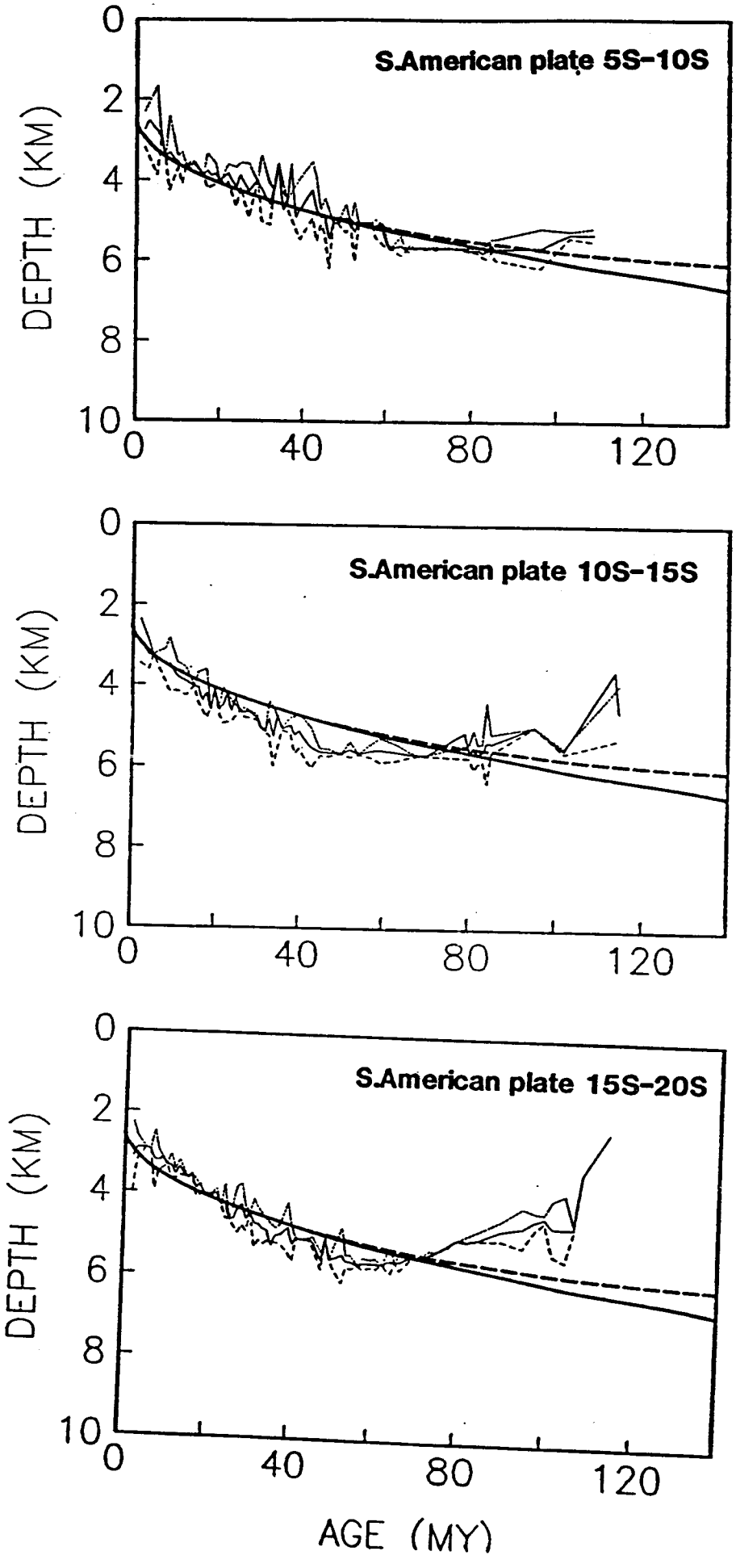
S.American plate 5S-10S
S.American plate 10S-15S
S.American plate 15S-20S
DEPTH (KM)
0
2
4
6
8
10
0
40
80
120
AGE (MY)

Fig. 15

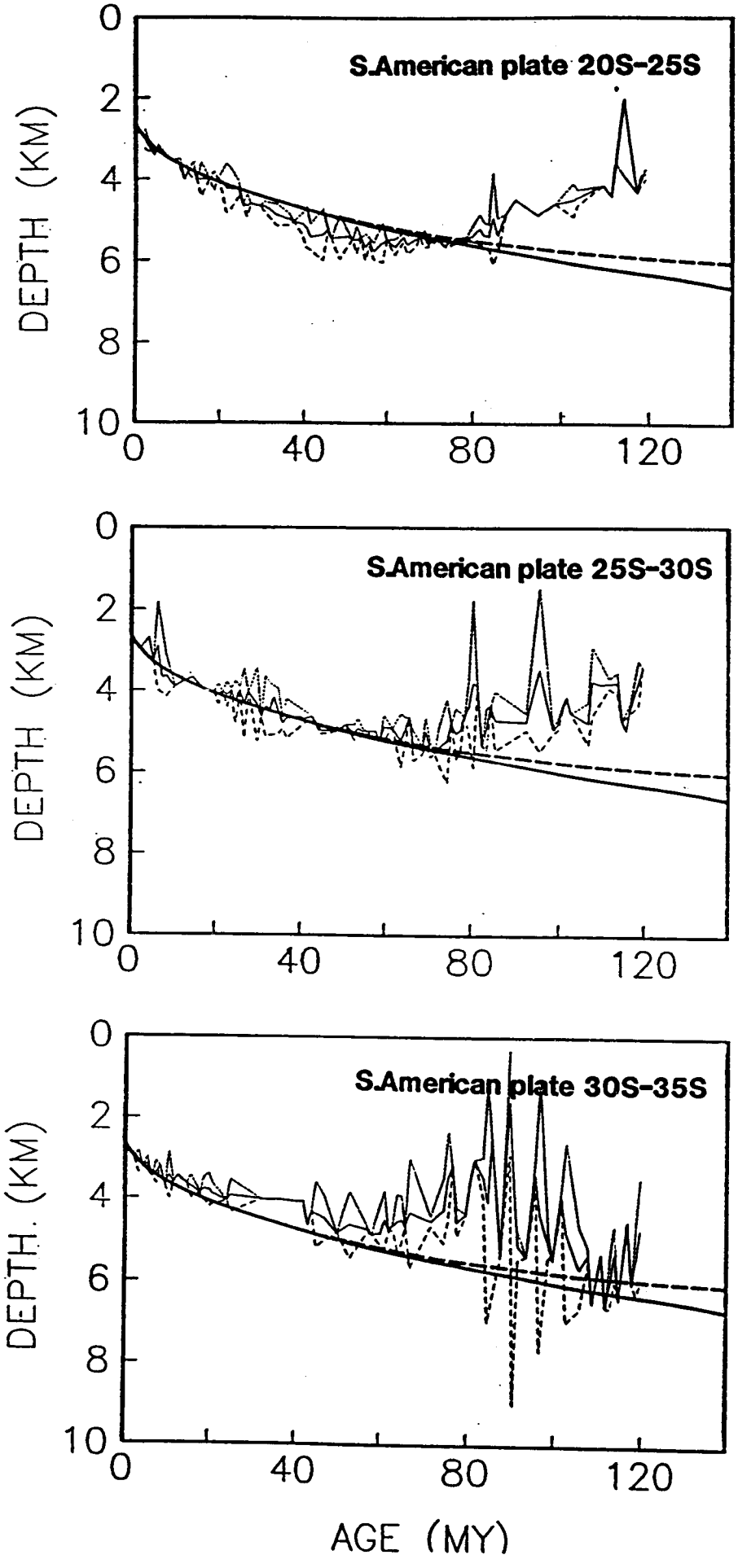

Fig. 15 continued

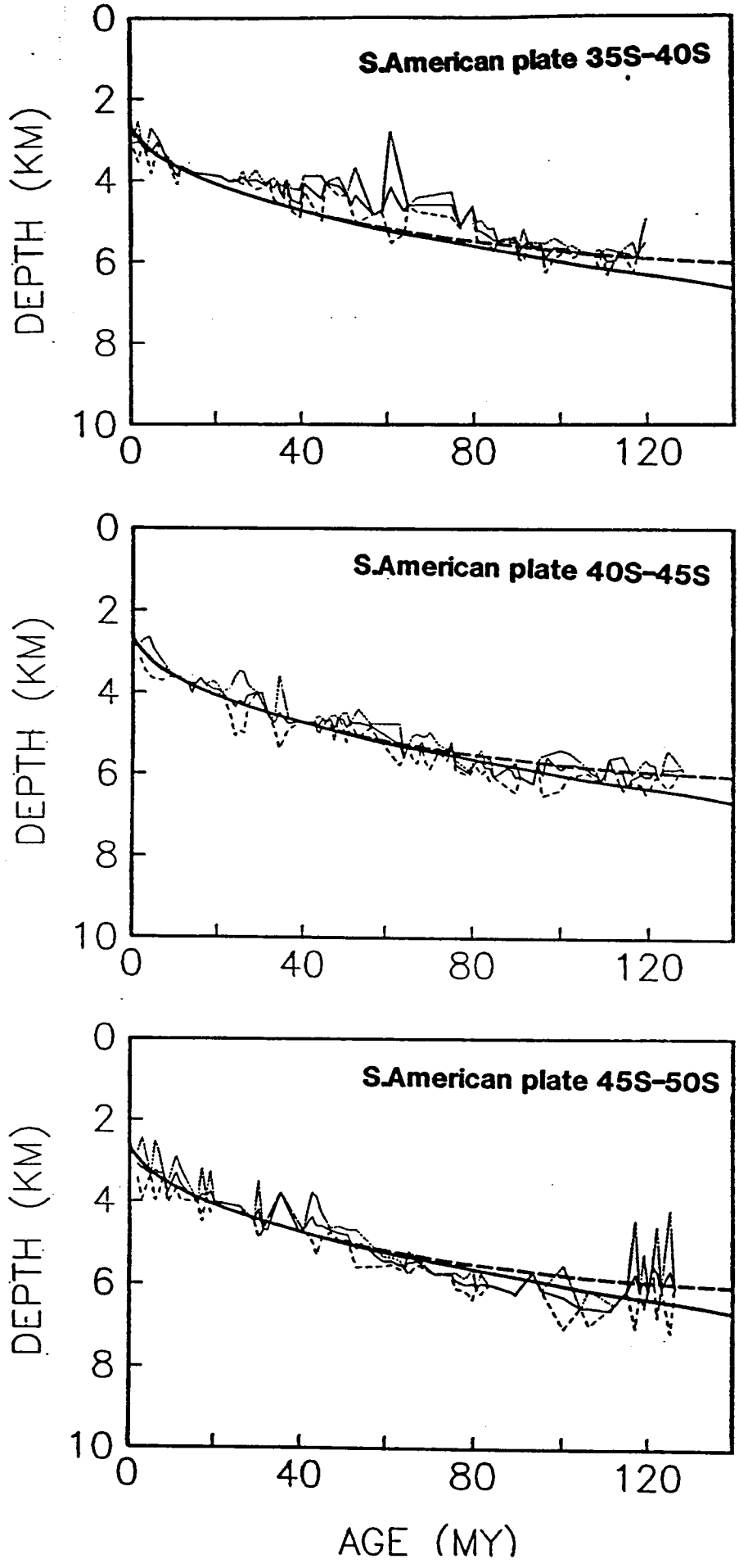

Fig. 15 continued

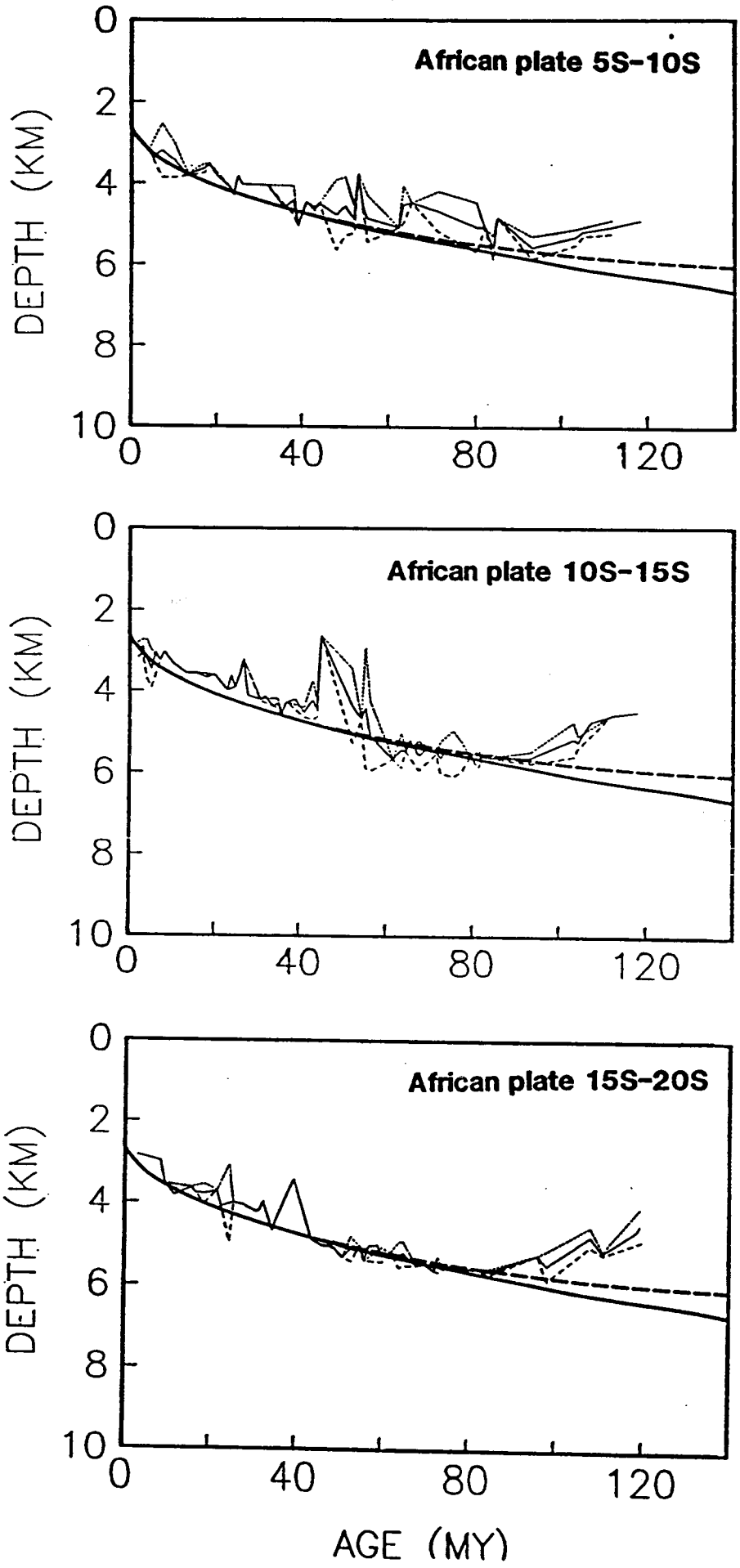
African plate 5S-10S
African plate 10S-15S
African plate 15S-20S
DEPTH (KM)
0
2
4
6
8
10
0
40
80
120
AGE (MY)

Fig. 16

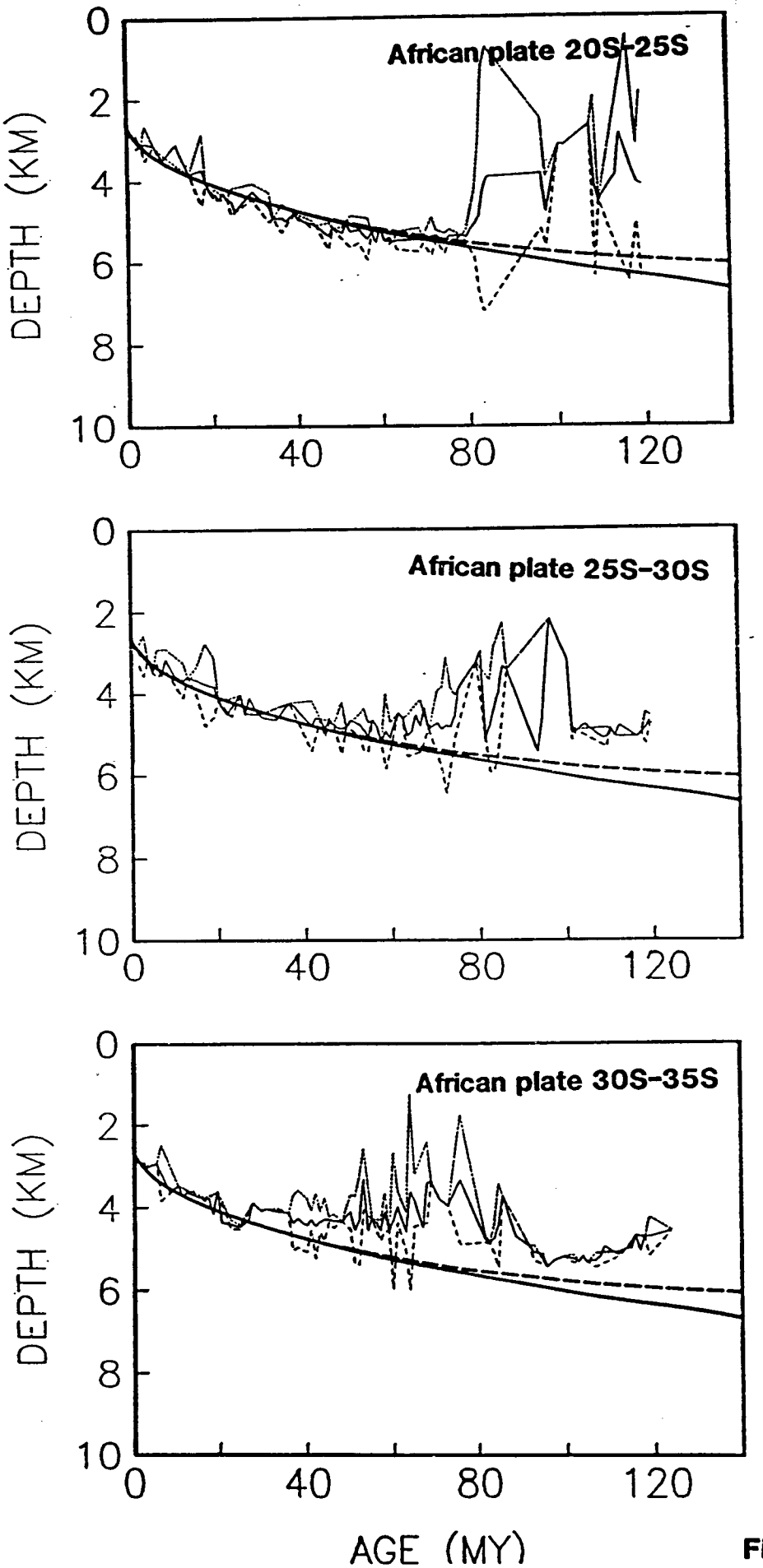

Fig. 16 continued

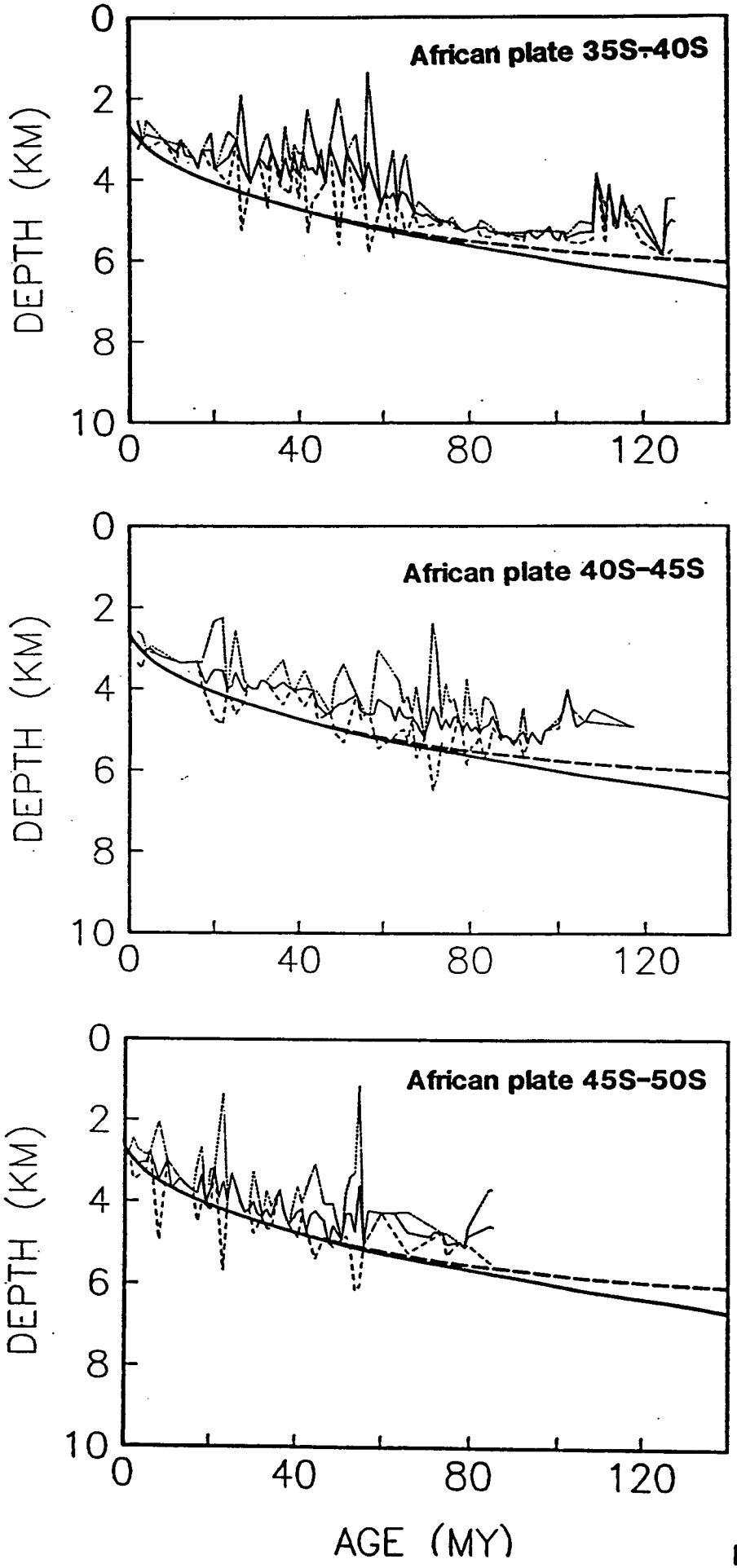

Fig. 16 continued

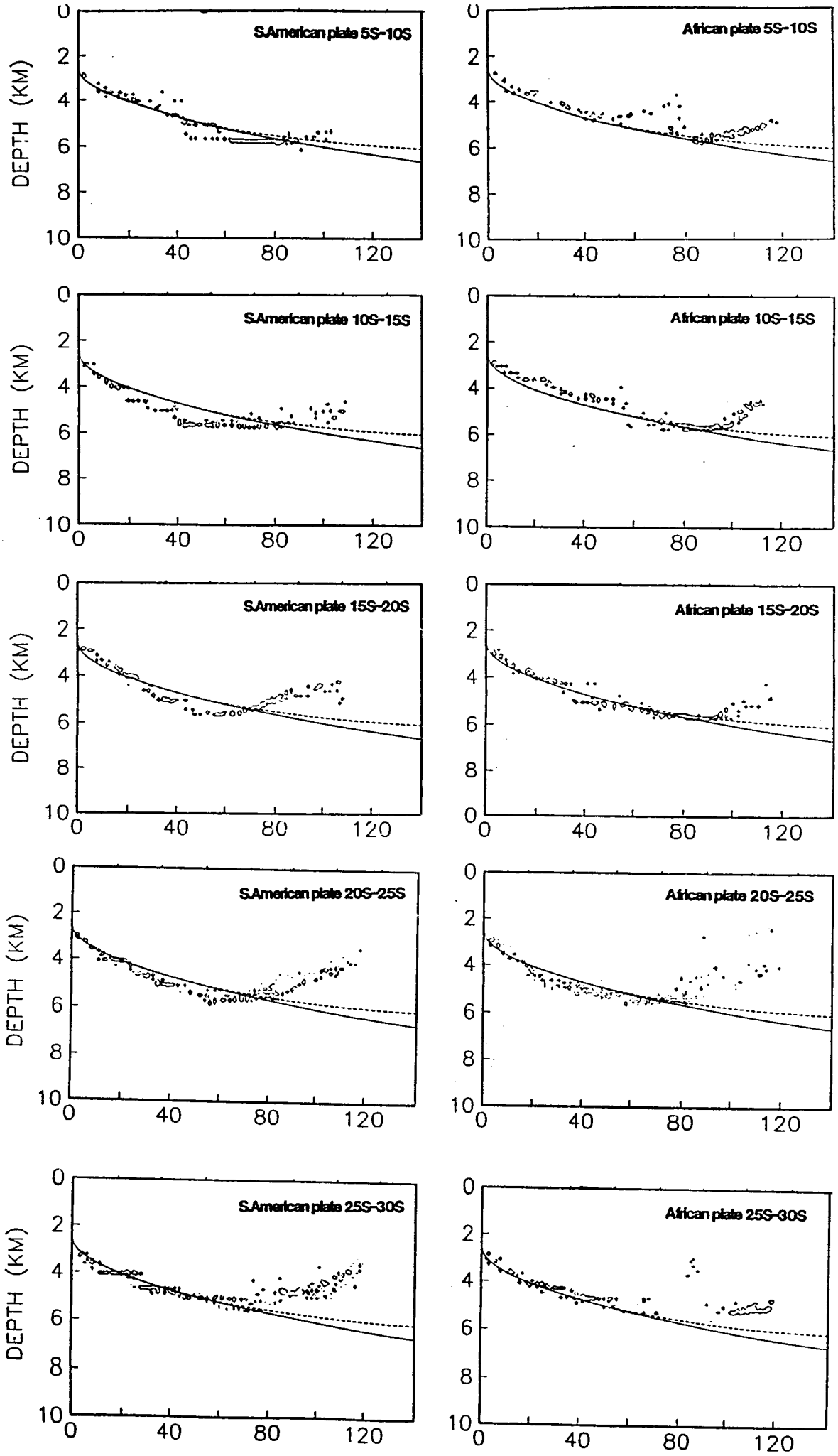
SAmerican plate 5S-10S
African plate 5S-10S
SAmerican plate 10S-15S
African plate 10S-15S
SAmerican plate 15S-20S
African plate 15S-20S
SAmerican plate 20S-25S
African plate 20S-25S
SAmerican plate 25S-30S
African plate 25S-30S
DEPTH (KM)
0
2
4
6
8
10
0
40
80
120

Fig. 17

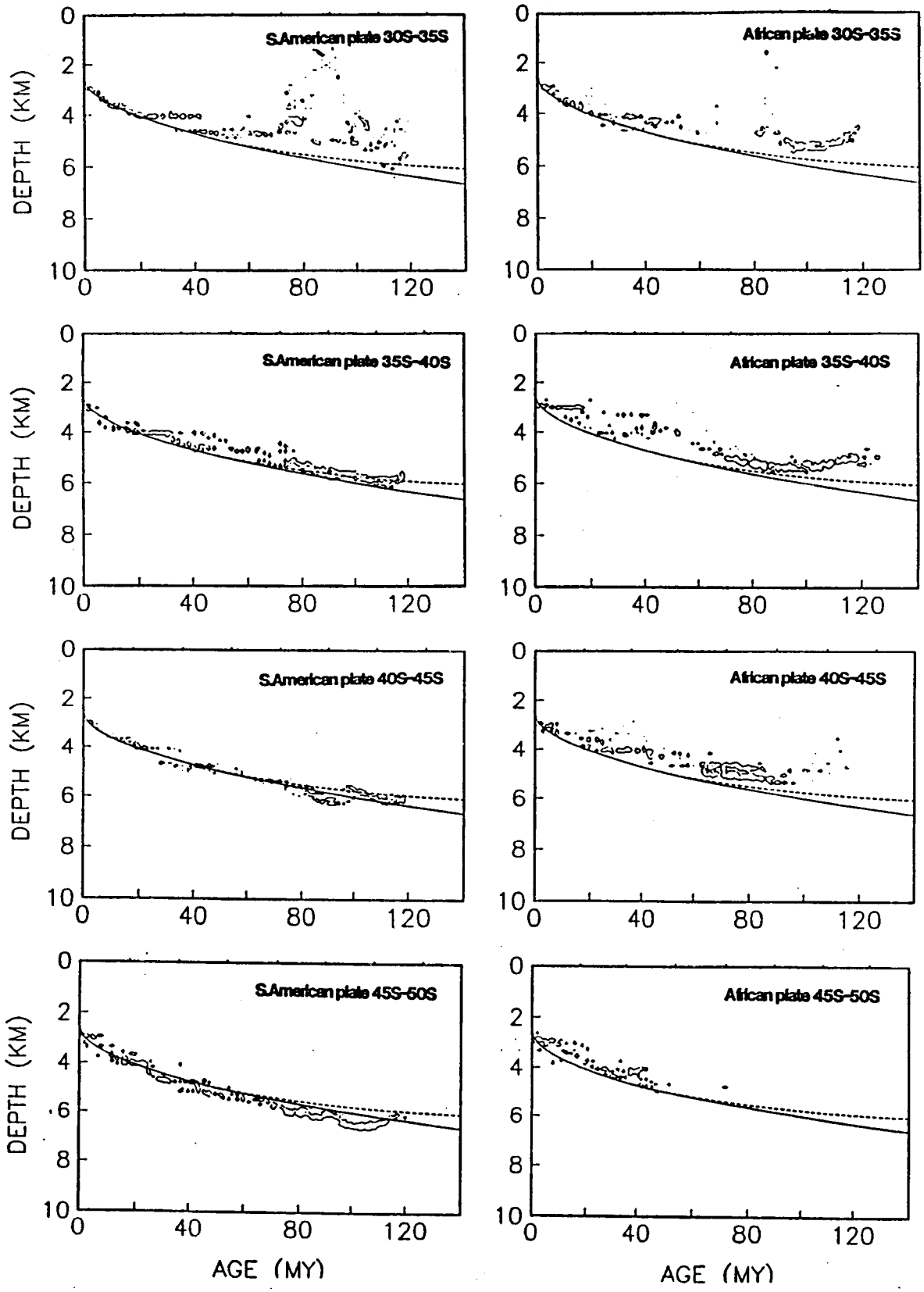

Fig. 17 continued

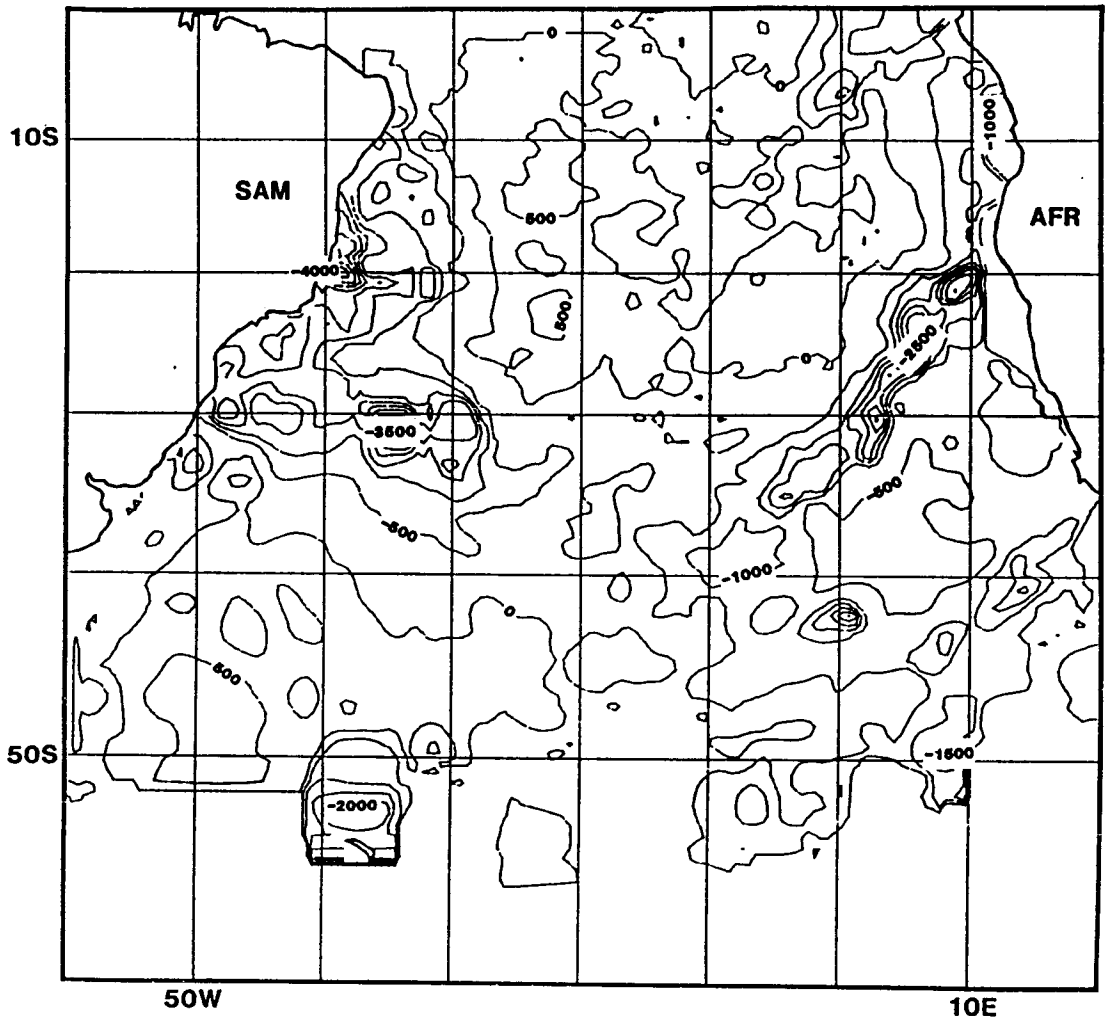
10S
50S
50W
10E
SAM
AFR
0
-1000
500
-4000
500
-2500
-3500
-500
-500
-1000
500
-1500
-2000

Fig. 18

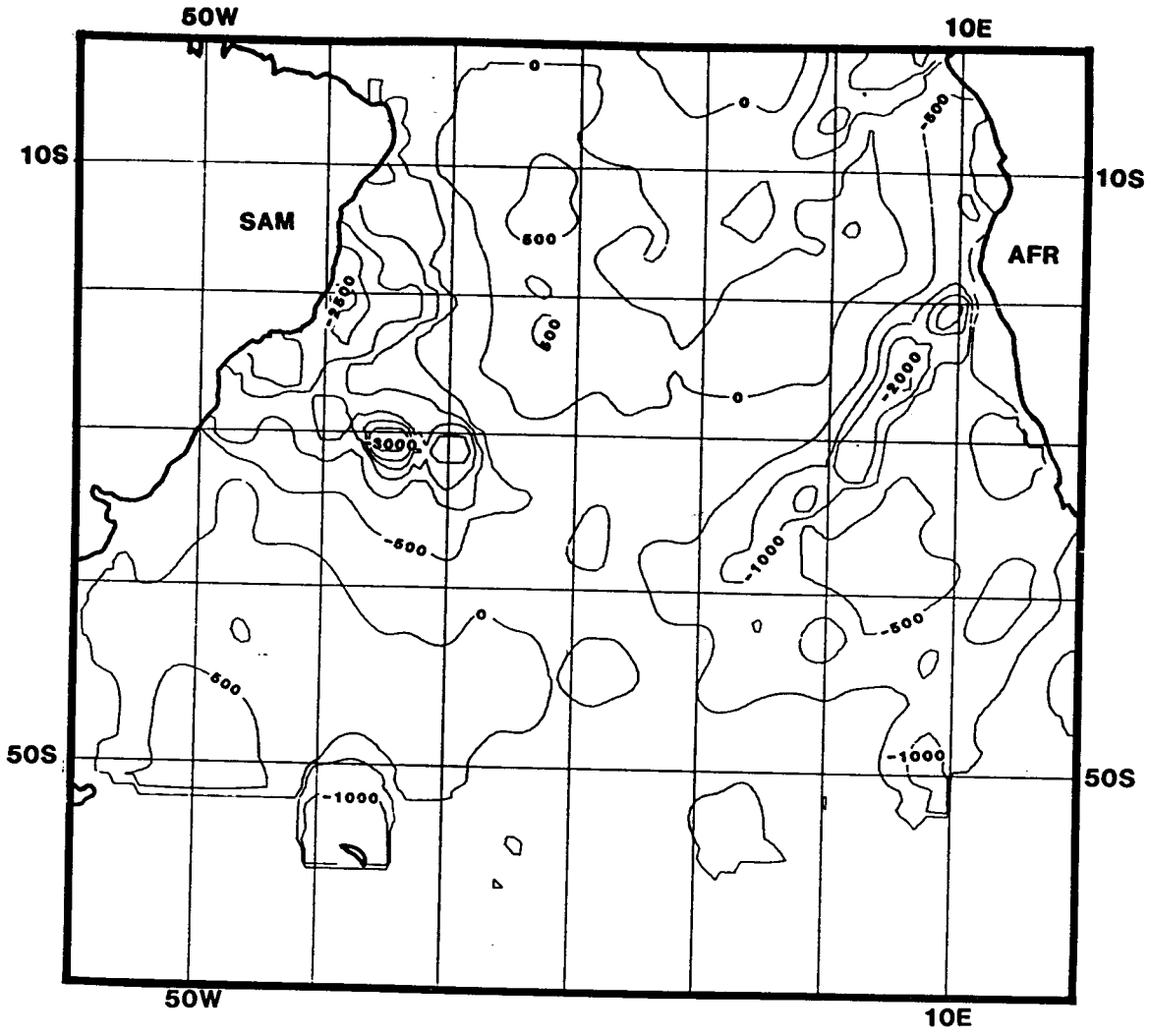
50W
10E
10S
10S
SAM
AFR
0
-500
-500
-2000
-3000
-500
-1000
0
-500
-500
50S
-1000
50S
50W
10E

Fig. 19

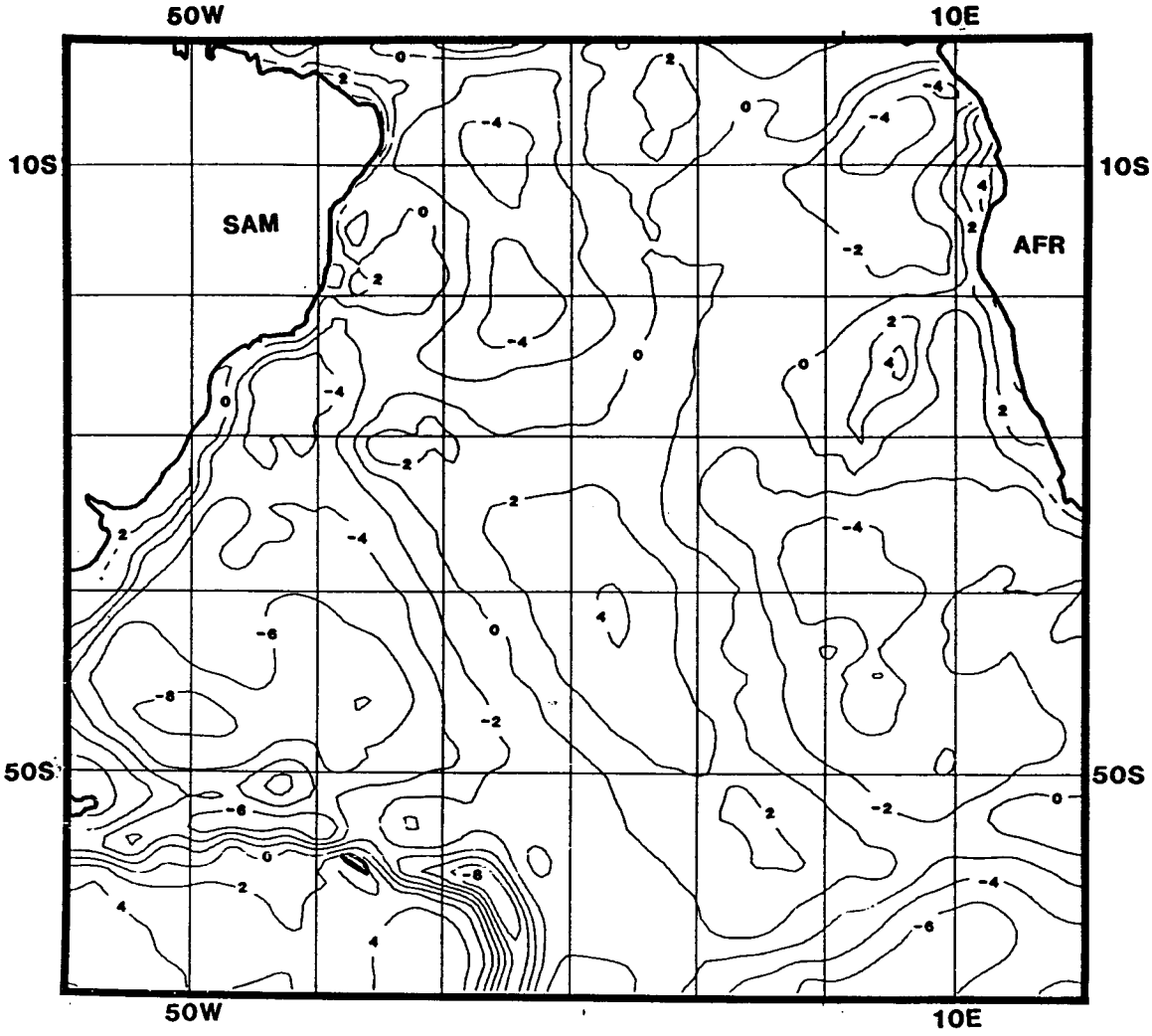

Fig. 20